Aus dem Institut für Diagnostische und Interventionelle Radiologie

der Universität Würzburg

Direktor: Univ.-Prof. Dr. med. Thorsten Bley

# Association of myocardial tissue characteristics and functional outcome in biopsy-verified myocarditis assessed by cardiac magnetic resonance imaging

Inauguraldissertation

zur Erlangung der Doktorwürde der

Medizinischen Fakultät

der

Julius-Maximilians-Universität Würzburg

vorgelegt von

Caroline Laqua

aus Estenfeld

Würzburg, Oktober 2023

## Referentenblatt

Referentin: Univ.-Prof. Dr. med. Bettina Baeßler

Korreferent: Univ.-Prof. Dr. med. Philipp Lurz

Dekan: Prof. Dr. Matthias Frosch

Tag der mündlichen Prüfung: 22.04.2024

Die Promovendin ist Ärztin.

# Table of content

# 1 Introduction

## 1.1 Myocarditis

Myocarditis means myocardial inflammation per se. The inflammatory process can also spread to the other heart wall layers, resulting in perimyocarditis or pancarditis. Myocarditis affects people of all ages and is the leading cause of heart failure in individuals under 40 years of age (1–5). In fact, myocardial involvement is estimated in up to five percent of all viral diseases, including the coronavirus disease 2019 (COVID-19) (6,7). The disease is likely to be underdiagnosed; thus, the worldwide incidence of up to 14 per 100,000 people per year might be considerably underestimated (2,8).

The causes of myocarditis can be very diverse. In Western civilization, it is most commonly caused by viral infections, often herpes viruses (e.g., Epstein-Barr virus, human herpesvirus type 6, human cytomegalovirus), coxsackieviruses of group A and B, and parvovirus B19 (9). Also, the novel coronavirus, severe acute respiratory syndrome coronavirus 2 (SARS-CoV-2) (10,11), and vaccination against it (12) can lead to myocarditis. Other potential pathogens are staphylococci, streptococci, Borrelia burgdorferi, several parasites, and fungal infections, the latter often in case of immunosuppression. Autoimmune diseases, radiation, and toxic substances such as medicaments, cytostatic drugs, heavy metals, and alcohol are known to be non-infectious causes of myocarditis (9). For more detailed information on the causes of myocarditis, please refer to Table 1.

Concerning pathophysiological processes in typical acute myocarditis, damage to cardiomyocytes is based on the pathogen itself, the body's immune response to it, and potentially resulting autoimmunologic reactions. The disease can become chronic if pathogens are not entirely eliminated or the immune response does not stop (13). The predominant type of infiltrating cells in the myocardium is used to classify myocarditis histopathologically into lymphocytic, granulomatous, eosinophilic, and giant-cell myocarditis (2).

Regarding the course of the disease, acute, fulminant, subacute, or chronic forms of myocarditis can be distinguished, albeit with heterogeneous definitions and fluent transitions between these (2,13). Table 2 summarizes the different forms of myocarditis.

**Table 1. Causes of myocarditis, modified according to Lampejo et al. and Caforio et al.** (2,14)

| | |
|---|---|
| **Infections** | |
| | e.g., herpes viruses (e.g., Epstein-Barr virus, human herpesvirus type 6, human cytomegalovirus), enteroviruses (e.g., coxsackieviruses A and B), adenoviruses, parvovirus B19, severe acute respiratory syndrome coronavirus 2 (SARS-CoV-2) and human immunodeficiency virus-1 (HIV-1) |
| Bacterial | e.g., Staphylococcus, Streptococcus, spirochaetes (e.g., Borrelia burgdorferi), Pneumococcus, Meningococcus, Haemophilus influenzae, Mycoplasma pneumoniae |
| Fungal | e.g., Aspergillus, Actinomyces, Blastomyces, Candida, Cryptococcus, Histoplasma |
| Protozoal | e.g., Toxoplams gondii, Trypanosoma cruzi, Entamoeba |
| Parasitic | e.g., Echinococcus granulosus, Taenia solium, Trichinella spiralis |
| Rickettsial | e.g., Rickettsia rickettsiae |
| **Toxins** | |
| Drugs | e.g., amphetamines, cocaine, ethanol, anthracyclines, chemotherapeutics (e.g., cyclophosphamide, fluorouracil, trastuzumab), lithium, catecholamines, interleukin 2 |
| Animal bites and stings | e.g., by scorpions, snakes, bees, wasps, spiders |
| Physical pathogens | e.g., radiation |
| Heavy metals | e.g., iron, copper |
| **Immune-associated causes** | |
| Allergic | e.g., vaccines, antibiotics, anticonvulsants |
| Transplant rejection | e.g., after heart or stem cell transplantation |
| Systemic autoreactive disorders | e.g., systemic lupus erythematosus, rheumatoid arthritis, rheumatic heart disease, Kawasaki's disease, scleroderma, polymyositis, myasthenia gravis, insulin-dependent diabetes mellitus, thyrotoxicosis, sarcoidosis, granulomatosis with polyangiitis |

Prognosis generally depends on etiology, initial clinical presentation, and the disease's course. The global overall mortality rate ranges between 1% to 7%. In the United States

of America, about 75% of hospitalized patients with myocarditis showed an uncomplicated course of the disease, along with an average mortality rate of 0%. Within patients presenting with complications, such as ventricular arrhythmias or acute heart failure, 12% either needed heart transplantation or died inside the hospital (8). Up to 30% of patients with preceding biopsy-proven myocarditis develop permanent cardiac dysfunction due to dilated cardiomyopathy (DCM), associated with poor prognosis (2,9,14).

**Table 2. Clinical forms of myocarditis** (2,13)
DCM = dilated cardiomyopathy

| Form of myocarditis | Clinical characteristics |
|---|---|
| **Acute myocarditis** | ● < 1 month between symptom onset and diagnosis<br>● Various symptoms and types of clinical presentation |
| **Fulminant myocarditis** | ● Severe form of acute myocarditis<br>● Possibly life-threatening complications (e.g., cardiogenic shock, cardiac arrhythmia, sepsis) |
| **Subacute myocarditis** | ● 1 – 3 months between symptom onset and diagnosis<br>● Symptoms either due to continuous myocardial injury or in the course of gradual healing |
| **Chronic myocarditis** | ● Symptoms lasting > 1 month (partly overlap with subacute forms)<br>● Development of long-term consequences (e.g., DCM, severe heart failure, cardiac arrhythmias) possible |

For patients with uncomplicated myocarditis, outpatient care is usually sufficient. Resting without physical exercise for at least six months is essential for a full recovery. In contrast, patients presenting with uncertain diagnosis or complicating factors should be admitted to the hospital to be diagnosed and monitored, respectively. Identifying a specific cause in patients with myocarditis is often impossible. Myocarditis in the Western civilization is most commonly caused by viral infections which are usually treated by supportive therapy, if necessary. However, in some cases, it is possible to determine the damaging agent. In case of infection, patients should be administered an anti-infective medication, either antibiotics, antimycotics, or virostatics. Immunosuppressive therapy may be an option to cure some autoimmune forms, e.g., myocardial inflammation coinciding with rheumatologic diseases or cardiac sarcoidosis (14,15). Regarding the therapy scheme, myocarditis in patients with COVID-19 makes an exception. These patients need to be treated with glucocorticoids if they are hemodynamically impaired or

present with coincident COVID-19 pneumonia and need supportive oxygen therapy (16). An appropriate medical therapy according to the guidelines for heart failure is indicated in case of impaired cardiac function. If not hemodynamically stable, patients require admission to the intensive care unit to be treated with inotropic and anti-arrhythmic drugs or mechanical circulation support, e.g., veno-arterial extracorporeal membrane oxygenation (VA-ECMO), if necessary. For therapy-resistant myocarditis patients with severe arrhythmias or heart failure, implantation of left ventricular assist devices (LVAD) or heart transplantation are the ultimate treatment options (2,8).

Myocarditis can present with multiple symptoms. In most cases, it passes either asymptomatically or with mild symptoms, including unspecific complaints such as headaches, myalgia, feelings of vertigo, fever, fatigue, and reduced performance. On the other hand, patients might also report acute chest pain (82% to 95% of adult patients with acute myocarditis), dyspnea (19% to 49%), palpitations, and syncope (5% to 7%) (8). If the chest pain is breathing-dependent, it might indicate a pericardial involvement. Moreover, infectious myocarditis is frequently related to preceding viral infections, e.g., airway infections, so asking about a patient's medical history over the past six months is necessary.

Different types of myocarditis can be distinguished depending on the predominant clinical presentation (17). They are described in Table 3.

**Table 3. Clinical presentation of myocarditis** (17)

ECG = electrocardiogram, LV = left ventricular

| Infarct-like myocarditis | Cardiomyopathic or Heart failure-like myocarditis | Arrhythmic myocarditis |
|---|---|---|
| ● Resembles acute coronary syndrome<br>● Chest pain, increased serum troponin I, elevated ST segments in ECG, and facultative fever | ● Resembles other forms of cardiomyopathy<br>● Severe LV dysfunction<br>● No serum marker anomalies or ECG changes | ● Resembles other forms of severe arrhythmias<br>● Sudden, often life-threatening ventricular arrhythmias<br>● No signs of infection or inflammation |

Separating myocarditis from other disease entities with similar clinical presentation can be extremely challenging (2,5,15,18,19). Thus, it is crucial to rule out a relevant coronary artery disease by computer tomography (CT) or invasive coronary angiography to differentiate it from infarct-like acute myocarditis during the early phase of clinical management.

Diagnosis of myocarditis involves several diagnostic criteria [cf. Diagnostic criteria for clinically suspected myocarditis by the European Society of Cardiology (ESC) (14)], summarized in Table 4 (14). According to these criteria, myocarditis can be suspected

in the presence of at least one of the stated symptoms and at least one diagnostic criterion, and the simultaneous absence of relevant coronary artery stenosis (≥ 50%) and other cardiovascular or extra-cardiac causes for the symptoms or abnormalities.

**Table 4. Criteria for diagnosing clinically suspected myocarditis by the European Society of Cardiology (ESC), modified according to Caforio et al.** (14)

AV = atrioventricular, ECG = electrocardiogram, LGE = late gadolinium enhancement, MRI = magnetic resonance imaging

| | |
|---|---|
| **A) Symptoms** | |
| ● Acute chest pain | Infarct-like or pericarditic (breathing-dependent) |
| ● Dyspnoea at rest or exercise and/or<br>● Fatigue, with/without<br>● Signs of heart failure | New-onset (< 3 months) or subacute/chronic (> 3 months) or worsening |
| ● Palpitation and/or<br>● Unexplained arrhythmia and/or<br>● Syncope and/or<br>● Aborted sudden cardiac death | |
| ● Unexplained cardiogenic shock | |
| **B) Diagnostic criteria** | |
| New abnormalities in<br>● ECG and/or<br>● Holter and/or<br>● Stress testing | Supraventricular tachycardia, I - III degree atrioventricular (AV) block, ST elevation or non ST elevation, T wave inversion, ventricular tachycardia or fibrillation and asystole, atrial fibrillation, reduced R wave height, widened QRS complex, abnormal Q waves, low voltage |
| ● Elevated serum markers for myocardiocytolysis | Troponin T, Troponin I |
| New abnormalities in function and/or structure on cardiac imaging:<br>● Echocardiogram and/or<br>● Angiography and/or<br>● Cardiac MRI | Regional wall motion or global systolic or diastolic function abnormality, with/without ventricular dilatation, with/without endocavitary thrombi, with/without pericardial effusion, with/without increased wall thickness |
| ● Cardiac MRI tissue characteristics | Myocarditis-typical pattern of edema and/or LGE |

In some North American and European countries, invasive endomyocardial biopsy (EMB) diagnosis remains the gold standard to confirm the clinical suspicion of

myocarditis. Additionally, analysis of the tissue gained by EMB might help determine the etiology and type of myocarditis and, thus, decide on the appropriate treatment, prognosis, and follow-up care. Although being an invasive procedure, complications due to EMB are scarce if conducted by an experienced interventional cardiologist (20–22). Nevertheless, there is always a risk of myocardial ischemia, arrhythmia, perforation of the heart wall with resulting pericardial tamponade, and bleeding with possible development of aneurysms at the puncture spot. Thus, EMB is not part of the routine practice for diagnosing myocarditis in most European countries, including Germany. Instead, it is only used in individual cases (14). EMB should comprise at least three samples, usually gained randomly from different spots of the myocardium and analyzed histologically and immunohistochemically. Also, polymerase chain reaction (PCR) for viral genomes can be performed. Repetition of EMB might be needed in a few cases to supervise response to treatment (14,23). However, the analysis of these few samples cannot certainly exclude the diagnosis of myocarditis since they might not represent the whole myocardium's histology. Consequently, sampling errors may occur.

Compared to EMB, cardiac magnetic resonance imaging (MRI) can offer various advantages. It is not invasive, and therefore, complications are rare. Moreover, the whole myocardium can be displayed and assessed. Thus, sampling errors are negligible in cardiac MRI.

Due to often inconspicuous or unspecific clinical symptoms, diagnosing myocarditis is extremely challenging, and sufficient therapeutical options are still limited. That explains the primary need for a reliable diagnosis. Cardiac MRI is a conclusive diagnostic tool regarding the presence or absence, localization, and severity of myocarditis.

## 1.2 Basics of magnetic resonance imaging

Felix Bloch and Edward Mills Purcell described the physical basis for MRI in 1945/46 for the first time (24). It is grounded on the nuclear spin of hydrogen nuclei (protons), which makes them magnetic. By applying a strong static homogenous magnetic field, the protons generate a longitudinal magnetization in the direction of the magnetic field. This magnetization is deflected from the direction of the static field and partially or fully converts into transversal magnetization if a radiofrequency alternating magnetic field is briefly applied in addition. The transversal magnetization starts to be in precession about the static magnetic field direction, i.e., it rotates. This precession motion of tissue magnetization induces an electrical tension that can be registered. After shutting off the high-frequency alternating magnetic field, transversal magnetization diminishes, so the

protons' spins align parallel to the static magnetic field again, called relaxation. For this relaxation, protons need a characteristic decay time that depends on the chemical compound and the molecular environment they are rotating in (25).

T1 relaxation, also called spin-lattice relaxation or longitudinal relaxation, is a disintegration constant describing the protons' returning to longitudinal magnetization. On the other hand, T2 relaxation, also called spin-spin relaxation or transverse relaxation, is a disintegration constant to describe the decay of the transverse magnetization after shutting off the radiofrequency impulse. These disintegration constants depend on the tissue and environmental characteristics and the method of measurement (25).

Regarding non-parametric MRI, the relaxation times and the content of hydrogen nuclei of different tissue types and the scanner's magnetic field, among other things, determine the signal intensity. Non-parametric MRI cannot quantify absolute relaxation times, so differences in signal intensities can only be interpreted in relation to other tissue types. Thus, high signal intensity is called hyperintense, meaning a tissue looks brighter than surrounding areas, and low signal intensity is called hypointense (25). In T1-weighted images, fluids appear hypointense, while in fat-suppressed T2-weighted images, fluids, e.g., edema, appear hyperintense (26).

Parametric MRI has several advantages over non-parametric imaging since it depicts absolute relaxation times for each voxel. That quantifiability reduces the signal intensity's dependence on other parameters and the subjective nature of image interpretation, improving intra- and interobserver variability and comparability between different patients or scanners (23).

Gadolinium is the contrast agent used in MRI to make blood circulation visible. In hyperemic tissue, a strong circulation causes early flooding with contrast agents [early gadolinium enhancement (EGE)]. In contrast, necrotic, fibrotic, edematous, or scarred tissues show poor circulation due to expanded extracellular volume, so the gadolinium-based contrast agent is flooded in and washed out lately [late gadolinium enhancement (LGE)] (26).

## 1.3 Cine MRI and feature tracking for assessing myocardial strain

The myocardial strain serves as a quantitative marker for the regional function of the myocardium. Numerous cardiac diseases do not involve the heart as a whole in the early stages but are limited to regional impairments in separate myocardial segments. Global measures, like the heart's ejection fraction (EF), are thus less likely to catch early

dysfunction (27–29).

Cine imaging is a technique of non-parametric cardiac MRI. It aims to capture the heart's motion during the cardiac cycle. For cine MRI, data is acquired throughout the cardiac cycle using an ECG-synchronized gradient echo sequence, typically by balanced steady-state free precession (bSSFP). Breath-holding during data acquisition is required to avoid additional motion artifacts. Finally, the images are reconstructed from the average of multiple heartbeats (30,31).

Feature tracking (FT) is a postprocessing method for time-resolved (cine) cardiac MRI that allows the reproducible regional quantification of cardiac wall motion (measured as strain) along different orientations (longitudinal, radial, circumferential) over the whole heart cycle (32,33).

The myocardial strain ($\varepsilon$) describes the displacement of points in the myocardium at a specific time in the cardiac cycle relative to its original distance (usually end-diastolic):

$$\varepsilon\,[\%] = \Delta l / l_{end-diast.}$$

where $\Delta l$ is the relative change in myocardial length between end-diastole and end-systole, and $l_{end-diast.}$ is the end-diastolic myocardial length (34). By convention, the Green-Lagrange formulation is used in cardiac imaging to define the myocardial strain (35).

The strain is separated into circumferential, longitudinal, and radial components according to the spatial directions, as shown in Figure 1. The circumferential and the longitudinal strain describe the shortening parallel to the endomyocardial border in the short axis (SAX) and long axes (LAX) planes, respectively. Thus, they have a negative algebraic sign. The radial strain is the relative lengthening perpendicular to the former two directions and has a positive sign (cf. Figure 1) (27).

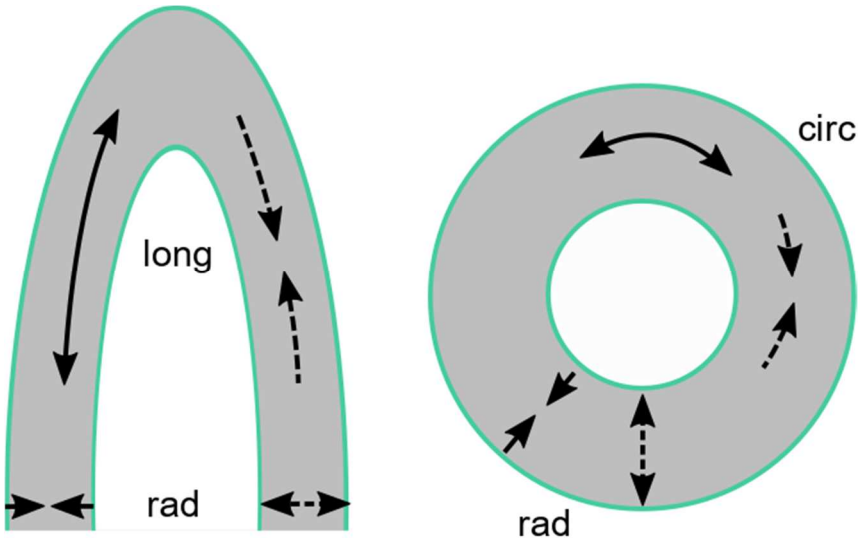


**Figure 1. Schema of the myocardial strain components, modified according to Almutairi et al.** (27)

On the left side, the longitudinal and radial myocardial deformation are shown in the heart's LAX view. On the right side, the circumferential and radial myocardial deformation are shown in the heart's SAX view. Dashed lines represent the systolic deformation, and solid lines the diastolic deformation.

circ = circumferential, LAX = long axes, long = longitudinal, rad = radial, SAX = short axis

## 1.4 MRI parametric mapping

Amongst others, parametric MRI comprises the techniques of T1 and T2 mapping. For each voxel, the respective relaxation time is calculated as a constant in an exponential decay process described by Bloch's equations (24). T1 maps are calculated from a co-registered series of images acquired at varying times from an inversion or saturation pulse. A series of images from a turbo-spin-echo sequence with varying echo times is acquired to calculate T2 maps. Thus, MRI mapping can exhibit regional myocardial T1 or T2 values for each voxel instead of presenting relative signal intensities as non-parametric MRI does (23,36–38). That makes it possible to distinguish between different tissue types and characteristics, such as edema or fibrosis, in mapping sequences (25). Figure 2 exhibits T1- and T2-weighted cardiac MRI sequences in comparison to T1 and T2 maps.

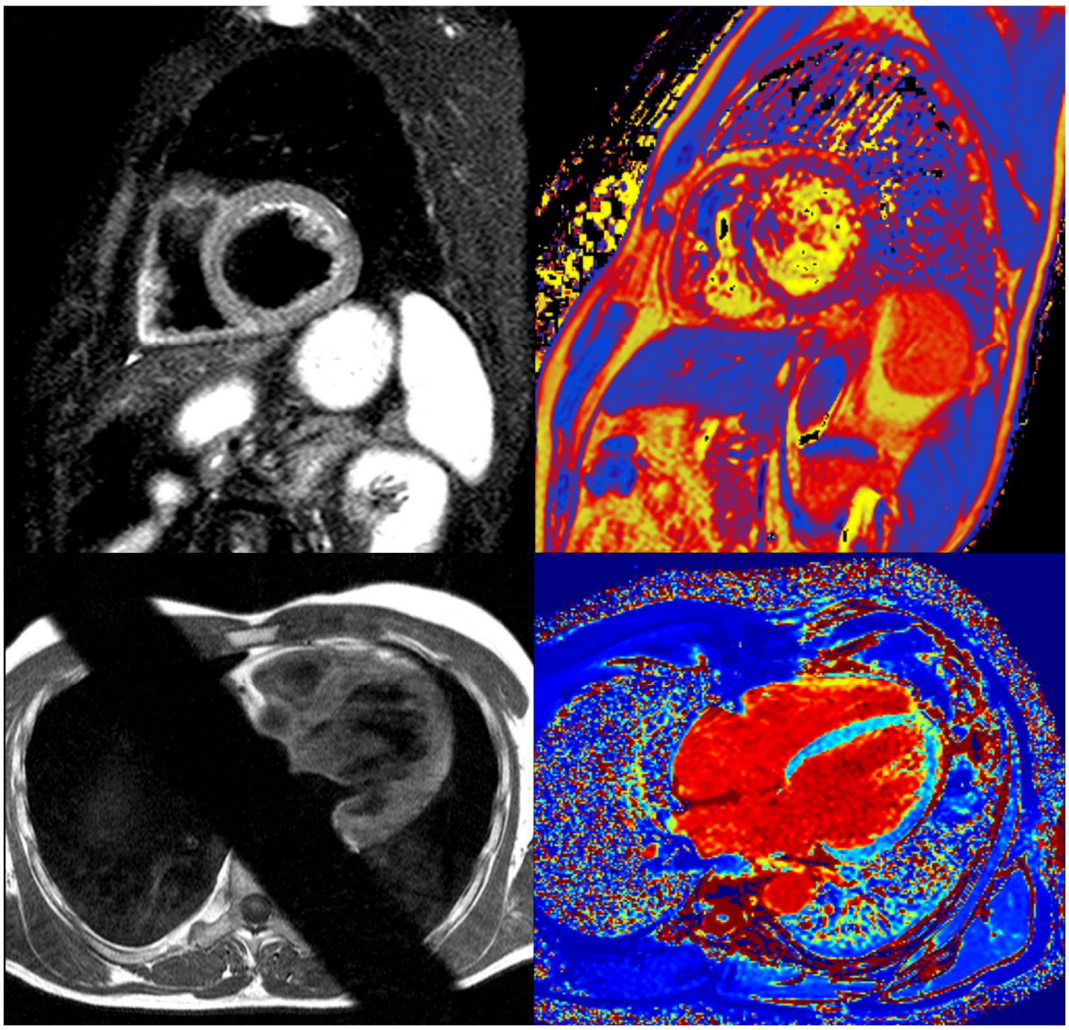

**Figure 2. Non-parametric in contrast to parametric cardiac MRI**

The top left corner shows a T2-weighted cardiac MRI sequence in SAX view, top right corner shows a T2 map in SAX view, the bottom left corner shows a T1-weighted sequence in horizontal long axis-view, and the bottom right corner shows a T1 map in horizontal long axis-view. MRI maps are derived images, calculated from a stack of images with varying acquisition parameters and color-coded for regional T1 and T2 values, respectively.

MRI = magnetic resonance imaging, SAX = short axis

## 1.5 Cardiac MRI in myocarditis

### Nomenclature for myocardial segmentation in cardiac tomographic imaging

In contrast to prior studies (18,32,39–41), the present work focuses not only on the global myocardial peak strain but also on the regional distribution of the heart's wall motion. To calculate the regional peak strain, we divided the LV myocardium into 17 segments

according to the nomenclature for myocardial segmentation in cardiac tomographic imaging stated by the Cardiac Imaging Committee of the Council on Clinical Cardiology of the American Heart Association (AHA) (42).

For this purpose, the cardiac planes used in heart imaging were named SAX, vertical long axis, and horizontal long axis. In echocardiography, the vertical long axis displays the left atrium and LV, analogous to the 2-chamber (2Ch) plane. The horizontal long axis displays all four heart chambers like the 4-chamber (4Ch) plane in echocardiography. Below, we call the cardiac planes SAX, 2Ch, and 4Ch for good comprehensibility, whereby 2Ch and 4Ch have collectively been described as LAX in this work.

Perpendicular to the heart's long axis, the LV is divided into a basal, midventricular, and apical third for AHA segmentation. The LV's basal SAX slice consists of the myocardial AHA segments 1 to 6, the midventricular slice of AHA segments 7 to 12, and the apical slice of AHA segments 13 to 16, as shown in Figure 3. AHA segment 17 is located in the heart's apex (cf. Figure 3) (42).

### Diagnosing myocarditis in cardiac MRI

In the past decade, cardiac MRI has emerged as the reference standard for the non-invasive detection of myocardial inflammation in patients with suspected myocarditis so that invasive examinations like EMB or coronary angiography can often be avoided (2,43).

Different cardiac MRI sequences based on T1 and T2 characteristics are qualified to depict the pathophysiological changes in the myocardium during inflammation: edema, hyperemia, and myocyte injury leading to necrosis and fibrosis. For this purpose, the Consensus Criteria for Cardiovascular Magnetic Resonance in Myocardial Inflammation, known as the "Lake Louise Criteria" (LLC), were established, and published in 2009 (26). Edema is displayed best in T2-weighted, hyperemia in EGE, and necrosis or fibrosis in LGE cardiac MRI, the three main criteria of the original LLC. According to signal intensities in the images, acute myocarditis has been deemed present if at least two of the three main LLC were positive. Additionally, systolic LV dysfunction and pericardial thickening or effusion indicating pericarditis in cine sequences of cardiac MRI (real-time MRI to capture the heart's motion) were considered for supporting the suspicion of myocardial inflammation (supportive criteria) (26).

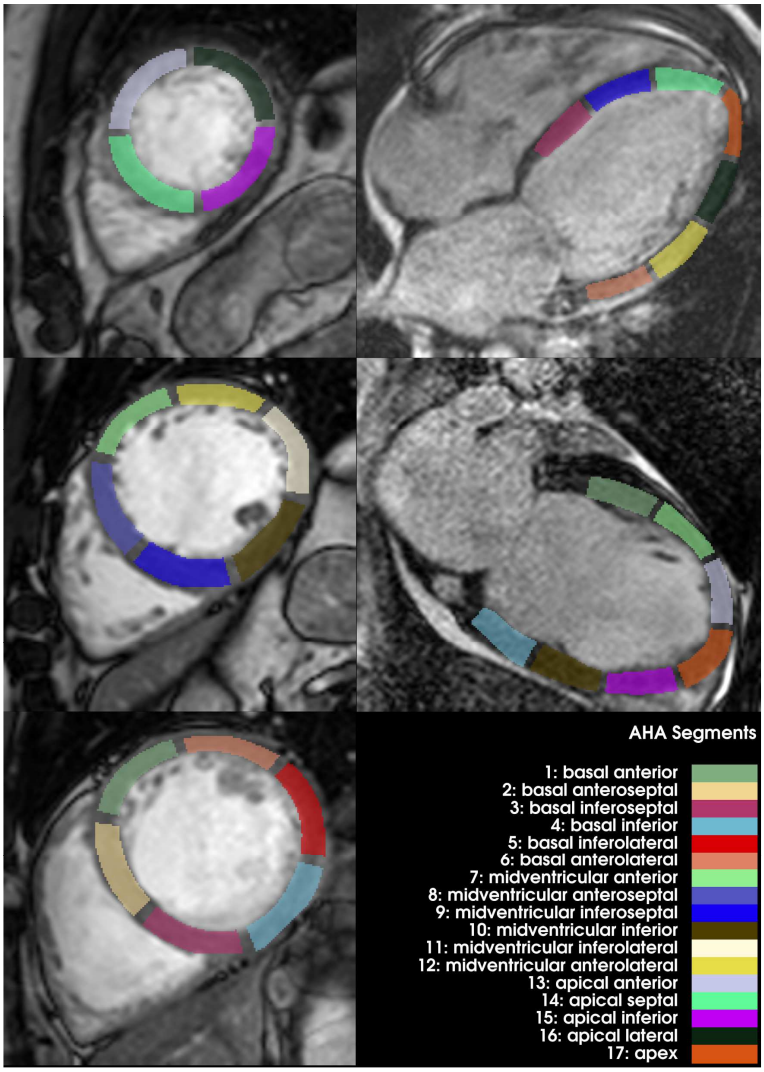


**Figure 3. Nomenclature and topography of myocardial segments in cardiac MRI according to the AHA** (42)

On the left side, the apical, midventricular, and basal layer of the heart's SAX view (from top to bottom) and their assigned myocardial segments are shown. On the right side, the 4Ch (on the top) and 2Ch (in the middle) planes with their assigned myocardial segments are shown. In the bottom right corner, a color-coded legend summarizes the names and numbers of the AHA segments.

AHA = American Heart Association, MRI = magnetic resonance imaging, SAX = short axis, 2Ch = 2-chamber, 4Ch = 4-chamber

However, after the technically advanced parametric mapping had been developed, the LLC were revised in 2018 (LLC II) (23) since numerous studies suggest that mapping techniques have a high sensitivity and specificity in assessing suspected myocarditis (36,44,45). The updated LLC (LLC II) consist of a T2-based marker for myocardial

edema and a T1-based marker for non-ischemic myocardial injury. Myocardial edema is supposed to be detected either in T2-weighted imaging or T2 mapping. Methods to identify myocardial injury can be LGE, T1 mapping, or extracellular volume (ECV) mapping. For instance, the ECV may be expanded in inflamed tissue due to edema or fibrosis. The supportive criteria comprise signs of pericarditis in cine images, LGE images, T1 or T2 mapping, and systolic wall motion abnormality of the LV in cine images. If at least one T1-based marker and one T2-based marker are positive for myocardial abnormalities combined with an appropriate clinical presentation, this ensures the diagnosis of myocarditis (23).

### Relation of MRI relaxation times to outcome in myocarditis

Moreover, cardiac MRI may also be of prognostic value (18,32,39–41). In patients suffering from myocarditis, appropriate risk stratification is important to determine the frequency and the extent of cardiological long-term follow-up since subclinical progression may occur and lead to DCM, ventricular dysfunction, heart failure, arrhythmia, or sudden cardiac death (14,40,46,47). In particular, the LV's global myocardial peak strain and LGE have been shown to be associated with adverse cardiac events and to independently predict all-cause and cardiac mortality (18,32,39–41).
However, literature on the relation of the myocardial peak strain and tissue characteristics to functional outcome (i.e., recovery of (left) ventricular function versus persistence of impaired function) is sparse (48,49). To our knowledge, it has yet to be discovered how the cardiac MRI tissue characteristics of myocardial edema (i.e., related to T1 and T2 relaxation times) and myocardial injury (i.e., related to T1 relaxation time) and their change over time are related to cardiac function. This research question relates to both global and particularly regional myocardial peak strain, edema, and injury.

## 1.6 Hypotheses of our work

We hypothesized

- that myocardial injury and myocardial edema in myocarditis (as quantified by T1 and T2 mapping, respectively) are associated with the regional myocardial peak strain in the respective segment (cross-sectional study),
- that a change in T1 and T2 relaxation times over time is related to recovery or worsening of myocardial function (functional outcome) quantified by the regional peak strain in this respective segment (longitudinal study), and

- that baseline T1 and T2 relaxation times are associated with a change in the (regional) myocardial peak strain over time (longitudinal study).

For this purpose, the baseline and follow-up cardiac MRI scans of the MyoRacer-Trial (45) were processed in FT and mapping analysis for each myocardial segment separately (cf. Figure 4).

# 2 Materials and Methods

## 2.1 Study design and population

Figure 4 gives a graphical abstract of our work. The following chapter describes our materials and methods in more detail.

All data of this work come from the MyoRacer-Trial, officially entitled “Myocarditis and the Role of Advanced Magnetic Resonance Imaging” (45). The MyoRacer-Trial was a prospective, observational study conducted from August 2012 to December 2015 at the Heart Center of the University of Leipzig, investigating 129 patients with clinically suspected myocarditis. The study intended to detect the diagnostic value of cardiac MRI compared to EMB as the established diagnostic gold standard (45,50). In our work, we reuse the MyoRacer-data to create a new substudy without any overlap with already published papers, taking a new contentual approach.

Study participants were between 18 and 80 years old and showed all sexes. Inclusion and exclusion criteria for patients with clinical suspicion of myocarditis are shown in Table 5 (45,50).

Within 36 hours after hospitalization, patients underwent systematic biventricular EMB, immuno-histological analyses, and comprehensive cardiac MRI on 1.5 Tesla (T) and 3 T scanners. On average, a follow-up (FU) 1.5 T cardiac MRI was performed three to four months after the baseline examination. Moreover, ten healthy subjects volunteered to undergo cardiac MRI to serve as a control group. The local ethics committee approved the study design, and all participants gave written informed consent. The full study protocol can be found at https://clinicaltrials.gov/ct2/show/NCT02177630 (5,45,50).

For our purposes, we excluded subjects with poor image quality or missing follow-up data. However, if only one specific sequence was insufficient or missing, the remaining data was still considered for statistical analysis. The absolute number of patients included in our analyses depended on the respective aspects of myocarditis in cardiac MRI. Please refer to the flowchart (cf. Figure 5) for more detailed information on the study population.

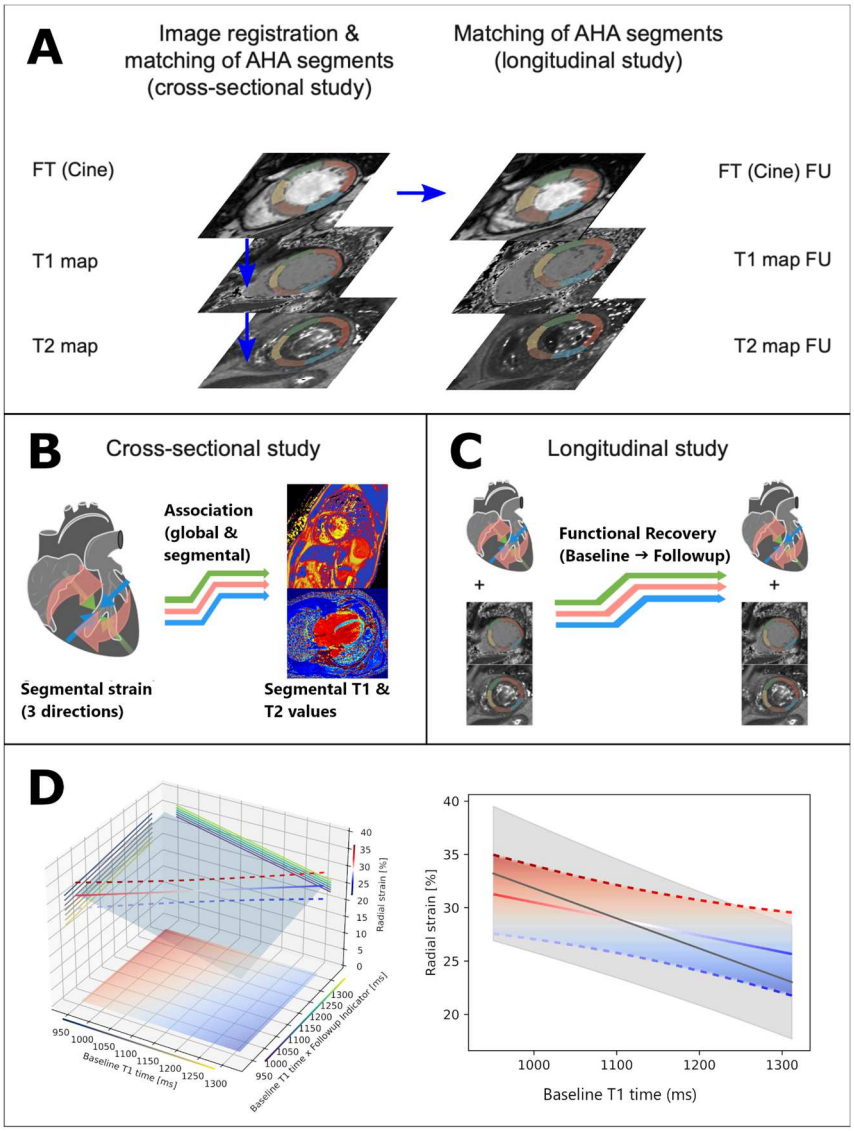


**Figure 4. Graphical abstract of study methods and key results**

A: We divided the LV myocardium in the MRI cine sequences into 17 segments and estimated the segmental myocardial strain using FT. Then, we registered T1 and T2 maps to the cine sequences and transferred the segmentations used for FT to ensure conformity of the myocardial segments.

B and C: Multi-level multivariable linear mixed effects regression was applied to investigate the relation of segmental myocardial strain to T1 and T2 relaxation times (B) and their respective change from baseline to follow-up (C).

D: Key results: The lower the baseline T1 time, the higher the radial peak strain at baseline. In contrast, the higher the baseline T1 time, the higher the recovery of radial strain at follow-up.

AHA = American Heart Association, FT = feature tracking, FU = follow-up, LV = left ventricular, MRI = magnetic resonance imaging

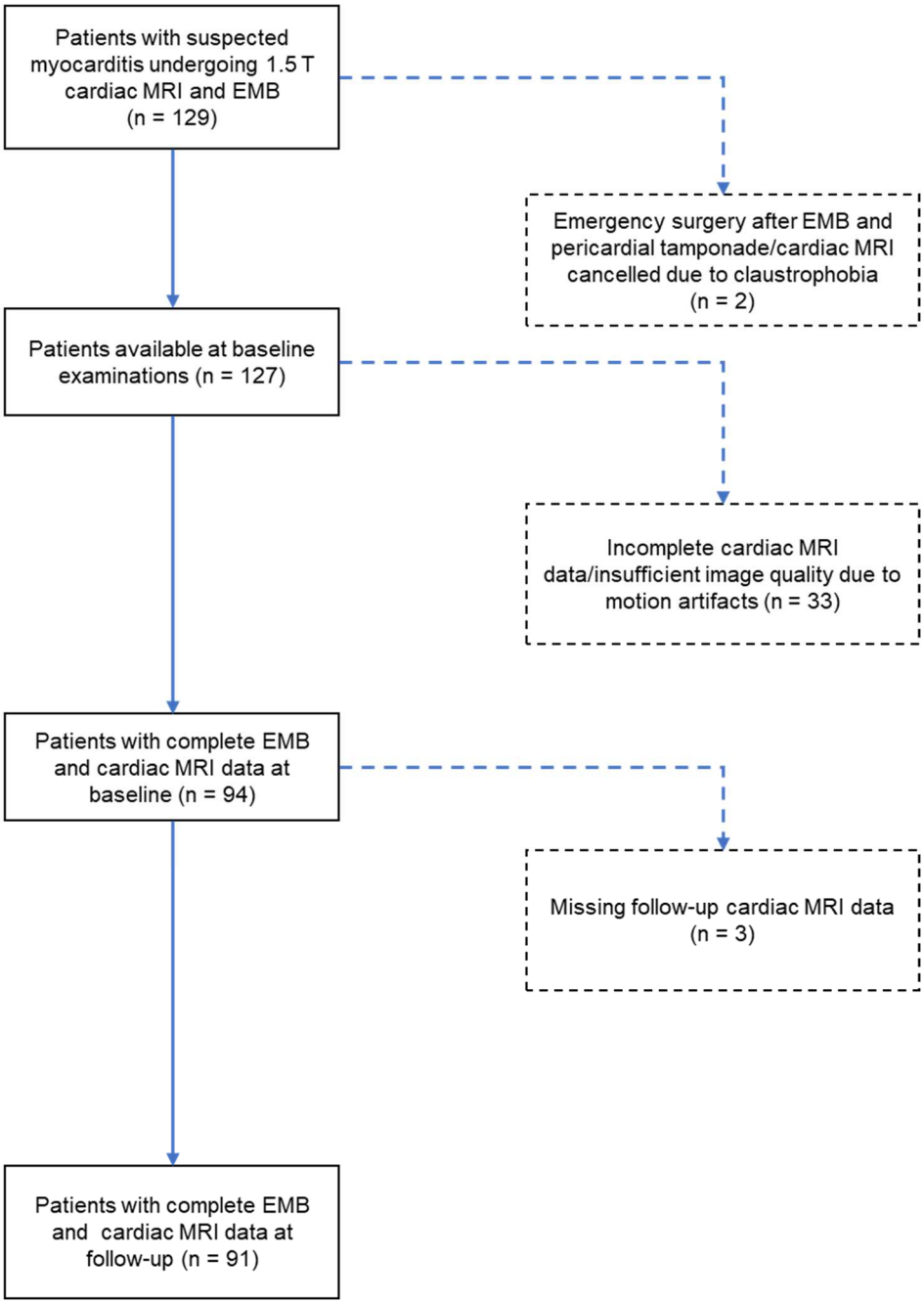


**Figure 5. Flowchart of the analytic sample of survey subjects' data** (5,45)

Study flow (on the left side) and reasons for participant dropout with numbers of excluded subjects (on the right side) are shown.

EMB = endomyocardial biopsy, MRI = magnetic resonance imaging, T = Tesla

**Table 5. Inclusion and exclusion criteria for participants in the MyoRacer-Trial** (45,50)

* Furthermore, subjects with nondiagnostic EMB or MRI were finally kept out of the statistical analysis (45).

ECG = electrocardiogram, EMB = endomyocardial biopsy, MRI = magnetic resonance imaging

| Inclusion criteria | Exclusion criteria * |
|---|---|
| Symptoms such as dyspnea or orthopnea, palpitations, exercise intolerance, fatigue, or angina pectoris | Relevant coronary artery disease on angiography |
| Evidence of myocardial involvement, namely ventricular dysfunction on echocardiography, new or persistent ECG changes, or elevated Troponin T | Contraindications to MRI, cardiac catheterization or EMB |
| History of systemic viral infection | Impaired renal function with a glomerular filtration rate ≤ 30 ml/min/m2 |
| | Pregnancy |
| | Missing informed consent |
| | Participation in another trial |

## 2.2 Endomyocardial biopsy and immunohistological analyses

An interventional cardiologist conducted angiography of the right and the left coronary artery to rule out a relevant coronary artery disease. EMB samples were taken from both ventricles. Five to seven samples were gained from the right ventricle (RV), mainly from septal or apical locations, while six to seven LV samples derived from different regions. Molecular pathological, histological, and immunohistological analyses were performed at the Department of Molecular Pathology, University Hospital Tuebingen (Tuebingen, Germany). PCR was conducted to detect viral genomes of adenoviruses, parvovirus B19, enteroviruses (including coxsackieviruses of group A and B and echoviruses), human cytomegalovirus, Epstein-Barr virus and human herpesvirus type 6 in cardiac tissue samples.

Myocarditis was diagnosed if at least 20 immune cells/mm2 infiltrating the myocardial tissue, like CD3+ T-lymphocytes or CD68+ macrophages, were present. We considered the detection of viral genomes without myocarditis as latent virus persistence. In contrast,

multifocal fibrosis or scarring in the absence of inflammation led to the diagnosis of healed myocarditis (5,45).

## 2.3 Cardiac magnetic resonance imaging

In our work, we analyzed cardiac MRI of a 1.5 T scanner (Intera, Philips, Best, The Netherlands) only because the follow-up examinations did not comprise a 3 T MRI (as baseline examinations did). The sequences were obtained with surface cardiac coils with five channels for the 1.5 T scanner. Table 6 reports non-parametric and parametric imaging parameters of the MyoRacer-Trial (5,45).

**Table 6. Non-parametric and parametric MRI parameters of the MyoRacer-Trial** (5,45)
bSSFP = balanced steady-state free precession, MOLLI = Modified Look-Locker inversion recovery, MRI = magnetic resonance imaging, SAX = short axis, TE = echo time, TI = inversion recovery time, TR = repetition time, 2Ch = 2-chamber, 4Ch = 4-chamber

| **Imaging parameters** | **Non-parametric imaging** | **Parametric imaging** | |
|---|---|---|---|
| | **Cine MRI** | **T1 mapping** | **T2 mapping** |
| Sequence type | bSSFP | MOLLI + bSSFP-readout | Turbo-Spin-Echo |
| Orientation | 1x 4Ch, 1x 2Ch, 10-14x SAX | 1x 4Ch, 1x 2Ch, 1x midventricular SAX | 1x 4Ch, 1x 2Ch, 1x midventricular SAX |
| Repetition time (TR) | 3.4 ms | 2.9 ms | 1052 ms |
| Echo time (TE) | 1.7 ms | 13 startup cycles to approach steady state, 8 echos (“3(3)5” scheme) | 9 echos (TE=13.2, 17.6, 21.9, 26.3, 30.7, 35.1, 39.5, 43.9, 48.3 ms) |
| Flip angle | 60° | 50° | 90° |
| Acquisition matrix | 1.25 x 1.25 mm² | 1.19 x 1.19 mm² | 0.96 x 0.96 mm² |
| Slice gap | 8 mm | - | - |
| Slice thickness | 8 mm | 10 mm | 8 mm |
| Inversion recovery time (TI) | - | 167 to 5472 ms | - |

### Calculation of T1 and T2 Maps

We applied an iterative motion correction and map fitting algorithm (51), adapted from Delso et al. (52):

First, the acquired raw mapping images were registered to a reference frame using the non-rigid Symmetric Normalization registration algorithm (53,54). Then, an initial map-fitting procedure was applied to the initial motion-corrected image set.

We applied the Levenberg-Marquardt algorithm to solve the 3-parameter exponential non-linear least-squares problems (52,55) pixel-wise in parallel. We implemented a pyramid architecture, where the weights of the subsequent cascade were initialized from a fit on a down-sampled dataset. After each iteration, the fitted model was used to generate synthetic images at all inversion recovery times (TI) and echo times (TE) for T1 and T2 mapping, respectively. The original images were then registered to the corresponding synthetic frame at the respective TI/TE. Afterward, we fitted a mapping model to the new motion-corrected image set. In total, we applied two iterations of this algorithm. We stored the pixel-wise $r^2$- values along with the T1 and T2 maps. The calculations were carried out on a high-performance computing cluster using the Tensorflow package (Version 2.6) in Python 3.8. More details on this novel method will soon be given in a separate manuscript that is currently in preparation (51).

## 2.4 Cardiac MRI analysis

### Myocardial strain analysis

FT-based strain analysis of the LV and RV was conducted using the commercially available software platform Segment (Version 3.3 R10187c, Medviso AB, Lund, Sweden, http://segment.heiberg.se) (56). This software uses deformable registration as the underlying FT method, and the reproducibility of segmental strain has been demonstrated (33).

Firstly, a study participant's cardiac MRI cine sequences (2Ch, 4Ch, SAX) were selected and loaded into the software. After that, we made the software automatically improve all sequences' image contrast. The next step was identifying each sequence's end-diastolic (ED) and end-systolic (ES) time points in the cardiac cycle. ED and ES time points were defined on a midventricular slice in the SAX view. Then, we automatically segmented the LV in the SAX view (57) and manually adjusted the myocardial contours if necessary. For the LV, there were two contours, the outer marking the line between epicardium and myocardium and the inner marking the line between myocardium and endocardium.

Afterward, FT analysis of the SAX could be initiated. For this purpose, we selected the heart's basal, midventricular, and apical slices and cropped the image to include the ventricles only. While waiting for the automatic registration process to be finished, we manually segmented the RV in the three slices of the SAX view. Then, we started working with the strain analysis module (58,59) for the SAX. Firstly, the marker for the allocation of the myocardial segments based on the standardized nomenclature of the American Heart Association (AHA) (42) had to be rotated to a mid-septal position in the midventricular layer. After that, we reviewed and adjusted the myocardial strain contours of LV and RV for optimal FT, if necessary.

In the last step, we processed the MRI cine sequences of the long heart axes (2Ch, 4Ch) by starting with the strain analysis module (58,59). Then, the images were cropped so that only the two or four heart chambers, respectively, were included. While waiting for the automatic registration process to complete, we manually segmented the LV in the 2Ch view and the LV and RV in the 4Ch view (56). Analogically to the SAX view, we plotted two myocardial contours for the LV and one for the RV. Finally, we reviewed and adjusted the myocardial strain contours for LV and RV for optimal FT in the strain analysis module (58,59) for 2Ch and 4Ch. Then, we saved the data file. We conducted the abovementioned process for each subject's baseline and follow-up cardiac MRI. Figure 6 shows an excerpt of the FT-based strain analysis in the software platform Segment (Version 3.3 R10187c, Medviso AB, Lund, Sweden, http://segment.heiberg.se) (56).

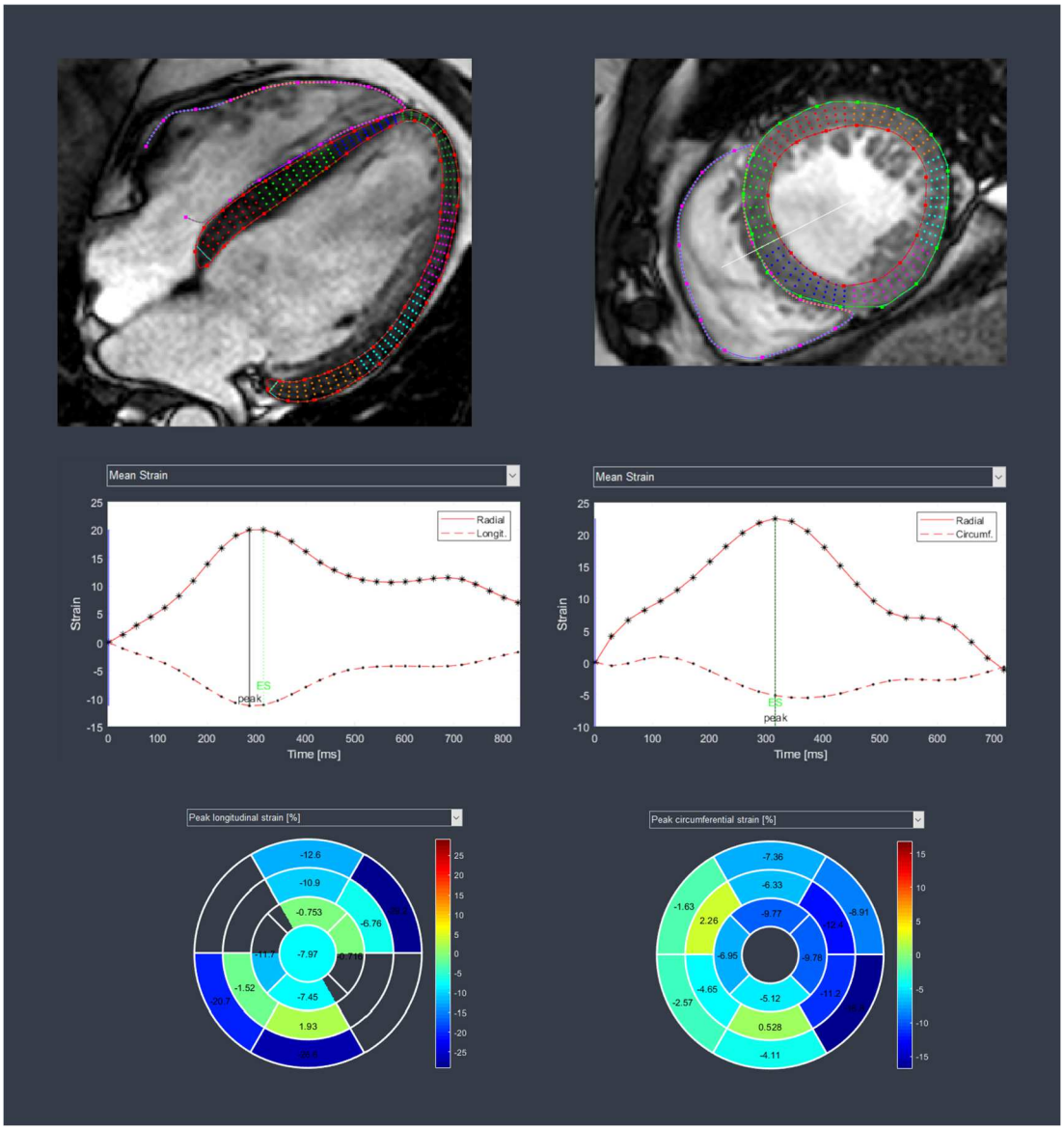


**Figure 6. FT-based strain analysis of the LV and RV using the software platform Segment** (Version 3.3 R10187c, Medviso AB, Lund, Sweden, http://segment.heiberg.se) (56)

On the right, the LV's and RV's strain analysis in 4Ch view, on the left, in SAX view are shown. At the top, the myocardial strain contours for FT are depicted, color-coded for the respective LV segments. In the middle, strain [%] over time [ms] curves can be seen. At the bottom, a bull's eye plot representing the LV myocardial segments shows the segmental peak longitudinal and peak circumferential strain, respectively.

FT = feature tracking, LV = left ventricle, RV = right ventricle, SAX = short axis, 4Ch = 4-chamber

### Assessment of myocardial tissue characteristics

To investigate the relation between myocardial tissue characteristics (i.e., myocardial edema and/or myocardial injury) and regional peak strain in each myocardial AHA segment, we needed to transfer the myocardial strain contours of the LV generated for FT to T1 and T2 maps. For this purpose, we used the free, open-source software 3D Slicer (Version 5.0.2 r30822 / a4420c3, Slicer Community, https://www.slicer.org/) (60). Myocardial tissue characteristics of the RV could not be depicted in MRI mapping since the RV myocardium layer is too thin. For the apical and basal layers in the SAX view, no T1 or T2 maps were available, either. Thus, the following explanations refer to the LV in the 2Ch view, 4Ch view, and the midventricular layer of the SAX view only.

### Coregistration of cine and mapping images

The end-diastolic cine images of all patients were automatically coregistered to the corresponding mapping images using a rigid transformation, followed by non-rigid Symmetric Normalization using antsRegistration (53,54). The delineated contours from Segment (Version 3.3 R10187c, Medviso AB, Lund, Sweden, http://segment.heiberg.se) (56) were extracted by a custom Python script, transformed into a segmentation map using the Simple Insight Toolkit Package (61), and warped to the domain of the coregistered mapping images. Here we preserved the AHA segments to match the segmental strain analysis to the mapping images. We applied automated binary manipulations to the segmentation (binary dilation and erosion (61)) and used them as a starting point for manual corrections in Slicer (Version 5.0.2 r30822 / a4420c3, Slicer Community, https://www.slicer.org/) (60). Figure 7 shows the close match of myocardial segmentation between cine images and cardiac MRI mapping and between MRI sequences from baseline and follow-up examinations.

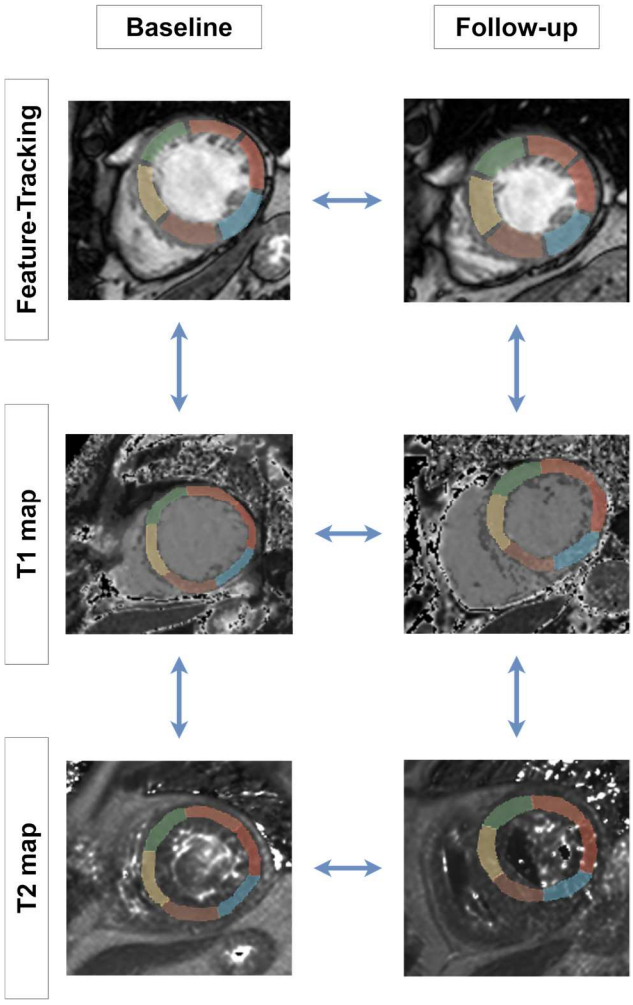


**Figure 7. Match of myocardial segmentation between the different cardiac MRI sequences in baseline and follow-up examinations in SAX view**

The location, orientation, and dimension of each color-coded myocardial segment are consistent in FT (cine) images, T1 and T2 maps, and in baseline and follow-up MRI. The segmental correspondence (represented by the double-headed arrows) was achieved by applying image registration, followed by human manual fine adjustment of the resulting transformed segmentations.

FT = feature tracking, MRI = magnetic resonance imaging, SAX = short axis

### Manual correction of mapping segmentations

In the first step, we manually applied a translation and rotation to ensure that the strain silhouette and the myocardium in the map would lay one above the other. Then, we adjusted the width and length of the myocardial segments to the depicted myocardium in the mapping images. That way, we ensured that the segment contours only covered myocardial tissue and left out the pericardium and the ventricle's lumen. Finally, we saved the data file. We conducted this process for each subject's T1 and T2 maps for baseline and follow-up cardiac MRI.

### Extraction of segmental T1 and T2 relaxation times

We applied the resulting segmental label masks to the T1 and T2 maps and calculated a weighted average in the respective segments. The weighted average accounts for errors in the map fitting procedure. Here, every pixel's T1 and T2 value was weighted by its corresponding $r^2$- value in the range of 0.9 to 1. For every pixel with an $r^2$- value below 0.9, the weight "0" was assigned, and hence it was excluded from the calculated average in this segment.

## 2.5 Statistical analysis

### Baseline characterization of study population

We provide mean (standard deviation) for continuous and count (relative percentage) for the study population, respectively. Here, we compared the population by EMB result using the Kruskal-Wallis test for continuous and Fisher's exact test for binary variables, respectively.

### Multi-level mixed effects linear regression

We fitted two-way/three-way linear mixed-effects regression models to model the relation of T1 and T2 time with myocardial radial, longitudinal, and circumferential peak strain. The general equation for this model is given by:

$$y_{strain} = X \cdot \vec{\beta}_{fixed} + Z_{patient,(segment)} \cdot \vec{u}_{random} + \epsilon$$

- $X \cdot \vec{\beta}_{fixed}$ describes the fixed effects (i.e., constant across all patients/segmentations)

- The term $Z_{patient,(segment)} \cdot \vec{u}_{random\ intercept}$ describes the random intercepts for the individual patient (and for the segmental analysis also the hierarchical level of the AHA segment).
- $\epsilon$ is the (normal-distributed) residual term.

*Association of positive EMB result with recovery of myocardial peak strain [model i)]*

For addressing the systematical effect of the follow-up period and the result of the EMB (cf. Table 8), we included fixed effects for the follow-up-indicator $k$ [i.e., the binary variable indicating whether an observation is from baseline ($k$=0) or follow-up ($k$=1)] and the indicator of a positive EMB result $EMB\_res$:

$$X \cdot \vec{\beta}_{fixed} = k \cdot \beta_k + EMB\_res \cdot \beta_{EMB\_res} \left(+EMB\_res \times k \cdot \beta_{EMB\_res \times k}\right)$$

We applied the likelihood ratio (LR) test to test for a potential interaction $EMB\_res \times k$ between both covariables.

*Cross-sectional association of T1 and T2 relaxation times with myocardial peak strain [model ii)]*

For cross-sectional regression on the relaxation constants (T1 and T2, cf. Table 9), we added fixed slopes for the relaxation constants and used fixed effects like in model i) to adjust for the EMB result and the follow-up indicator.

$$\begin{aligned} X \cdot \vec{\beta}_{fixed} = {} & T \cdot \beta_T \\ & + k_{follow-up} \cdot \beta_{follow-up} \\ & + EMB\_res \cdot \beta_{EMB\_res} \\ & \left(+EMB\_res \times T \cdot \beta_{EMB\_res \times T}\right) \end{aligned}$$

We tested for a potential effect-modification by the EMB result using the LR test on the interaction term $EMB\_res \times T$.

*Longitudinal association of peak strain recovery and change of relaxation times from baseline to follow-up [model iii)]*

For the effect of the change in relaxation time between baseline and follow-up (cf. Table 10), we split the relaxation constants into the sum of two variables: Baseline relaxation time $T_{baseline}$ and $\Delta T$, which is the difference between follow-up and baseline relaxation constants. In addition to the adjustments of model ii), we added fixed-effect coefficients for $T_{baseline}$ and $\Delta T$ (which is 0 for baseline records).

$$
\begin{aligned}
X \cdot \vec{\beta}_{fixed} \quad &= T_{\Delta T}\,[ms] \cdot \frac{\beta_{\Delta T}\,[\%/ms]}{\nu} \\
&+ T_{BL}\,[ms] \cdot \frac{\beta_{T_{BL}}\,[\%/ms]}{\nu} \\
&+ k_{follow-up} \cdot \beta_{follow-up} \\
&+ EMB\_res \cdot \beta_{EMB\_res} \\
&\left(+EMB\_res \times \Delta T \cdot \beta_{EMB\_res \times \Delta T}\right)
\end{aligned}
$$

Again, we tested for a potential effect modification by the EMB result using the LR test. In conclusion, the functional relationship for the myocardial peak strain at follow-up and baseline, respectively, is given by:

$$
\begin{aligned}
y_{strain}\left(\Delta T, k_{follow-up}\right)[\%] \quad &= \frac{\Delta T\,[ms]}{\nu} \cdot \beta_{\Delta T}\,[\%/ms] \\
&+ k_{follow-up} \cdot \beta_{follow-up} \\
&+ X_{other\ fixed-effects} \cdot \vec{\beta}_{other\ fixed-effects} \\
&+ Z_{patient,(segment)} \cdot \vec{u}_{random\ intercept} + \epsilon
\end{aligned}
$$

where

- $y_{strain}$ is the myocardial peak strain at follow-up or baseline, respectively.
- $\Delta T$ is the difference of the relaxation time at follow-up minus baseline.
- $\beta_{\Delta T}$ is the regression coefficient for the fixed-effect $\Delta T$ scaled by $\nu$ (100 for T1, 10 for T2).
- The term $Z_{patient,(segment)} \cdot \vec{u}_{random\ intercept}$ describes the random intercepts for the individual patient (and for the segmental strains also the AHA segment). Note that the adjustment for the baseline strain is contained in this term.
- Units are given in square brackets.

*Association of baseline relaxation times with functional recovery [model iv)]*

We modeled the association of baseline relaxation constant with the change of myocardial peak strain (cf. Table 11) by fixed effects for the peak strain at baseline, an indicator for baseline/follow-up, and an interaction term of the former and the latter.

$$
\begin{aligned}
X \cdot \vec{\beta}_{fixed} \quad &= T_{BL} \cdot \beta_{T_{BL}} \\
&+ k_{follow-up} \times T_{BL} \cdot \beta_{k_{follow-up} \times T_{BL}} \\
&+ k_{follow-up} \cdot \beta_{follow-up} \\
&+ EMB\_res \cdot \beta_{EMB\_res} \\
&\left(+EMB\_res \times k_{follow-up} \times T_{BL} \cdot \beta_{EMB\_res \times k_{follow-up} \times T_{BL}}\right)
\end{aligned}
$$

Here, we are mainly interested in the interaction term (second line) for the follow-up indicator and the baseline relaxation time. Its regression coefficient $\beta_{k_{follow-up} \times T_{BL}}$ gives the strength of the (adjusted) relationship of the baseline relaxation time and the functional recovery from baseline to follow-up.

We visually checked the model assumptions (linearity, homoskedasticity) by plotting the residuals.
An alpha level of 0.05 was considered the threshold for statistical significance.
No adjustment for multiple comparisons was implemented for this secondary explorative analysis in concordance with earlier arguments for this approach (62).
All statistical analyses were conducted in STATA 16.0 (StataCorp, Houston, Texas, USA) by Fabian Laqua.

# 3 Results

## 3.1 Baseline characteristics of study population

The study flow and reasons for participant dropout are shown in the “Flowchart of the analytic sample of survey subjects’ data” (cf. Figure 5 (5,45)).

Table 7 summarizes the main study participant characteristics at baseline examination (5,45). From 91 patients (cf. Figure 5) included in our analyses, 26 were EMB-negative for myocarditis, and 65 were EMB-positive. For study participants with a negative EMB result for myocarditis, the mean age was 46 ± 14 (standard deviation, SD) years, and 31% were female. The left ventricular ejection fraction (LVEF) was 36 ± 19 (SD) %, and the mean duration of symptoms was 47 ± 136 (SD) days in EMB-negative subjects.

EMB-positive study participants were 42 ± 15 (SD) years on average, and 26% were female. Their average duration of symptoms accounted for 61 ± 114 (SD) days, and the mean LVEF was 35 ± 17 (SD) %.

Apart from the immune cell count in EMB, classifying the study participants by definition as EMB-negative or EMB-positive, no statistically significant differences between these two groups were observed in the baseline characteristics (cf. Table 7).

**Table 7. Study participant characteristics at baseline, modified according to Lurz et al. and Baessler et al.** (5,45)

Values are given as mean (with standard deviation in brackets) for continuous data and as absolute count (with relative percentage in brackets) for binary data. We applied Fisher's exact and Kruskal-Wallis tests for binary and continuous variables, respectively. Units are given in square brackets. * $p < 0.05$ indicates statistical significance.

AV = atrioventricular, CK-MB = creatine kinase of the myocardium, ECG = electrocardiogram, EMB = endomyocardial biopsy, LV = left ventricular, LVEF = left ventricular ejection fraction, MRI = magnetic resonance imaging, NT-proBNP = N-terminal pro–B-type natriuretic peptide, RV = right ventricular, SAX = short axis, 2Ch = 2-chamber, 4Ch = 4-chamber

| Characteristic | EMB-negative (n = 26) | EMB-positive (n = 65) | p-value |
|---|---|---|---|
| Age [years] | 45.88 (14.09) | 42.32 (15.04) | 0.307 |
| Female sex | 8 (30.8%) | 17 (26.2%) | 0.795 |
| Viral anamnesis | 13 (54.2%) | 37 (58.7%) | 0.809 |
| Duration of symptoms [days] | 46.54 (135.93) | 61.12 (113.55) | 0.607 |
| Symptom | | | |
| Atypical chest pain | 8 (32.0%) | 24 (38.1%) | 0.632 |
| Angina | 4 (16.0%) | 19 (30.2%) | 0.281 |
| Dyspnoe | 16 (64.0%) | 40 (62.5%) | 1.000 |
| Fever | 3 (12.0%) | 14 (23.7%) | 0.373 |
| Edema | 5 (20.0%) | 8 (12.7%) | 0.506 |
| LVEF [%] | 35.92 (18.53) | 35.46 (17.01) | 0.911 |
| Troponin > 14 pg/l | 15 (65.2%) | 52 (83.9%) | 0.077 |
| CK-MB > 41 µmol/l | 4 (17.4%) | 23 (37.1%) | 0.116 |
| NT-proBNP [pg/ml] | 1971.20 (2593.58) | 2709.77 (4290.62) | 0.477 |
| Pathologies in ECG | | | |
| AV block | 3 (13.0%) | 14 (24.6%) | 0.368 |
| ST elevation | 0 (0.0%) | 4 (6.8%) | 0.313 |
| ST depression | 15 (68.2%) | 30 (51.7%) | 0.215 |
| Cardiovascular risk factor | | | |
| Hypertonus | 17 (68.0%) | 30 (47.6%) | 0.101 |
| Nicotine | 10 (41.7%) | 24 (40.0%) | 1.000 |
| Diabetes | 4 (16.0%) | 5 (7.9%) | 0.267 |
| Hyperlipoproteinemia | 8 (32.0%) | 20 (32.3%) | 1.000 |
| Adipositas | 11 (44.0%) | 29 (46.0%) | 1.000 |
| EMB result | | | |
| RV CD3+ cell count | 1.83 (0.92) | 10.51 (9.83) | <0.001* |
| RV CD68+ cell count | 8.91 (2.24) | 23.44 (12.98) | <0.001* |
| LV CD3+ cell count | 2.40 (0.80) | 13.89 (14.34) | <0.001* |
| LV CD68+ cell count | 9.54 (1.50) | 31.63 (21.97) | <0.001* |

**Table 7. Study participant characteristics at baseline, modified according to Lurz et al. and Baessler et al.** (5,45) **- Continuation**

| Characteristic | EMB-negative (n = 26) | EMB-positive (n = 65) | p-value |
|---|---|---|---|
| EMB result | | | |
| LV fibrosis [%] | 11.87 (7.63) | 10.83 (7.75) | 0.607 |
| RV fibrosis [%] | 9.11 (6.06) | 12.67 (10.11) | 0.147 |
| Cardiac MRI | | | |
| T1 time [ms] | 1116.7 (89.2) | 1147.9 (78.1) | 0.106 |
| T2 time [ms] | 60.2 (5.4) | 61.3 (4.4) | 0.339 |
| Average 2Ch longitudinal strain [%] | -10.8 (5.3) | -10.6 (4.6) | 0.837 |
| Average 4Ch longitudinal strain [%] | -10.8 (4.5) | -11.3 (4.2) | 0.651 |
| Average SAX circumferential strain [%] | -11.4 (5.6) | -11.6 (5.4) | 0.861 |
| Average 2Ch radial strain [%] | 21.6 (13.2) | 21.6 (12.6) | 0.980 |
| Average 4Ch radial strain [%] | 17.5 (9.8) | 19.0 (8.3) | 0.454 |
| Average SAX radial strain [%] | 21.9 (11.6) | 20.0 (10.0) | 0.437 |

## 3.2 Association of positive EMB result with recovery of myocardial peak strain [model i)]

Table 8 depicts the association of follow-up indicator [i.e., the binary variable indicating whether an observation is from baseline (= 0) or follow-up (= 1)] and EMB results with myocardial peak strain at baseline. The regression coefficients for the follow-up indicator give the average myocardial functional recovery. The algebraic signs of the regression coefficients determine the course of change in myocardial peak strain. For circumferential strain, a negative regression coefficient for the follow-up indicator means a higher absolute peak strain value at follow-up and vice versa (cf. Chapter 1.3).

A significant improvement in myocardial function from baseline to follow-up could be seen in all components of myocardial strain on the global and segmental levels (cf. Table 8). The absolute improvement ranged from 2.0% (global and segmental circumferential SAX peak strain) to 6.6% (global radial SAX peak strain) during the course of the disease (numbers are absolute changes; hence, percent is considered a unit). Overall, the EMB result did not significantly impact the myocardial peak strain at baseline. Only lower segmental radial SAX peak strain at baseline examination was significantly associated with biopsy-verified myocarditis. Furthermore, the likelihood ratio test for including an interaction term between the EMB result and the follow-up indicator did not provide significant evidence for an effect modification on the latter, i.e., functional recovery of the myocardium was not related to the EMB result.

**Table 8. Association of positive EMB result with recovery of myocardial peak strain [model i)]**

* p < 0.05 indicates statistical significance. † Wald's test whether the Reg. coef. equals 0. ‡ LR test for interaction between follow-up indicator [i.e., the binary variable indicating whether an observation is from baseline (= 0) or follow-up (= 1)] and EMB result (binary variable indicating a positive EMB result). Reg. coef. are adjusted for interindividual and intersegmental strain intercepts, and Reg. coef. for EMB results are additionally adjusted for follow-up. Units are given in square brackets.

CI = confidence interval, EMB = endomyocardial biopsy, LAX = long axes, LR test = likelihood ratio test**,** Reg. coef. = regression coefficient, SAX = short axis

| | Follow-up indicator | | | Positive EMB result | | | |
|---|---|---|---|---|---|---|---|
| **Myocardial peak strain [%]** | **Reg. coef.** | **95% CI** | **p-value Wald test †** | **Reg. coef.** | **95% CI** | **p-value Wald test †** | **LR test: p ($\chi^2$) ‡** |
| **Global circumferential SAX** | -2.018 | (-2.72;-1.32) | <0.001* | 0.376 | (-1.71;2.47) | 0.724 | 0.783 (0.076) |
| **Global radial SAX** | 6.57 | (4.82;8.32) | <0.001* | -2.905 | (-8.25;2.44) | 0.287 | 0.845 (0.038) |
| **Global longitudinal LAX** | -2.574 | (-3.08;-2.07) | <0.001* | -0.025 | (-1.84;1.79) | 0.978 | 0.724 (0.13) |
| **Global radial LAX** | 5.544 | (4.03;7.05) | <0.001* | 0.162 | (-3.78;4.10) | 0.936 | 0.743 (0.11) |
| **Segmental circumferential SAX** | -2.044 | (-2.45;-1.63) | <0.001* | 0.565 | (-0.38;1.51) | 0.243 | 0.598 (0.28) |
| **Segmental radial SAX** | 6.506 | (5.62;7.40) | <0.001* | -3.306 | (-5.55;-1.06) | 0.004* | 0.504 (0.45) |
| **Segmental longitudinal LAX** | -2.381 | (-2.81;-1.95) | <0.001* | 0.202 | (-0.53;0.93) | 0.59 | 0.677 (0.17) |
| **Segmental radial LAX** | 5.041 | (4.20;5.89) | <0.001* | -0.349 | (-1.86;1.16) | 0.651 | 0.547 (0.36) |

## 3.3 Cross-sectional association of T1 and T2 relaxation times with myocardial peak strain [model ii)]

Table 9 depicts the association of T1 and T2 relaxation times with the myocardial peak strain at one point in time (cross-sectional study). All baseline and follow-up data have been considered for the cross-sectional analyses, treating the follow-up data like separate (but clustered) samples to maximize the sample size. The regression coefficients quantify the absolute difference in myocardial peak strain per 100 or 10 ms difference in T1 or T2 relaxation time, respectively. Thus, the cross-sectional study results show the relation between peak strain and the respective relaxation time across different patients (interindividual variability). For circumferential strain, a positive regression coefficient means a lower absolute peak strain value in a patient with a T1 (T2) time 100 (10) ms higher than another patient's T1 (T2) time (cf. Chapter 1.3).

We found significant associations between increased T1 relaxation time and lower myocardial peak strain at one point in time in all segmental strain models and the models for global circumferential SAX peak strain and global radial SAX peak strain. The absolute difference in myocardial peak strain per 100 ms difference in T1 time ranged from 0.04% (global longitudinal LAX peak strain) to 2.6% (global radial SAX peak strain; numbers are absolute changes; hence, percent is considered a unit).

Increased T2 relaxation time was significantly related to lower global radial and longitudinal LAX peak strains and lower peak strains in all segmental models. Here, the absolute difference in myocardial peak strain per 10 ms difference in T2 time ranged from 0.4% (segmental circumferential SAX peak strain) to 2.0% (global radial LAX peak strain).

Overall, the EMB result did not significantly modify the effect of T1 and T2 relaxation times on myocardial peak strain (cf. Table 9 LR test for interaction between relaxation time and EMB result). Only for segmental radial LAX peak strain and T1 time, the likelihood ratio test for the interaction between relaxation time and EMB result provided significant evidence for an effect modification. I.e., the regression coefficients for this particular relation differed significantly between EMB-positive and EMB-negative patients.

**Table 9. Cross-sectional association of T1 and T2 relaxation times with myocardial peak strain [model ii)]**

* p < 0.05 indicates statistical significance. ✝ Wald's test whether the Reg. coef. equals 0. ‡ LR test for interaction between relaxation time and EMB result. Reg. coef. are adjusted for intraindividual differences in peak strain and T1 and T2 relaxation times, myocardial segments (in models with segmental strain), and EMB results (myocarditis or no myocarditis). Applied scaling factors: 100 for T1, 10 for T2. Units are given in square brackets.

CI = confidence interval, EMB = endomyocardial biopsy, LAX = long axes, LR test = likelihood ratio test, Reg. coef. = regression coefficient, SAX = short axis

| | | Relaxation time [ms] | | | |
|---|---|---|---|---|---|
| **Myocardial peak strain [%]** | | **Reg. coef.** | **95% CI** | **p-value Wald test ✝** | **LR test: T1\|2 x EMB result: p ($\chi^2$) ‡** |
| **Global circumferential SAX** | **T1** | 0.737 | (0.0025;1.47) | 0.049* | 0.602 (0.27) |
| **Global radial SAX** | **T1** | -2.578 | (-4.43;-0.73) | 0.006* | 0.613 (0.26) |
| **Global longitudinal LAX** | **T1** | 0.0435 | (-0.35;0.44) | 0.829 | 0.235 (1.41) |
| **Global radial LAX** | **T1** | -0.893 | (-2.01;0.22) | 0.117 | 0.514 (0.43) |
| **Segmental circumferential SAX** | **T1** | 0.568 | (0.26;0.88) | <0.001* | 0.452 (0.57) |
| **Segmental radial SAX** | **T1** | -1.889 | (-2.57;-1.21) | <0.001* | 0.493 (0.47) |
| **Segmental longitudinal LAX** | **T1** | 0.423 | (0.19;0.65) | <0.001* | 0.141 (2.17) |
| **Segmental radial LAX** | **T1** | -0.871 | (-1.32;-0.42) | <0.001* | 0.005* (7.95) |
| **Global circumferential SAX** | **T2** | 0.498 | (-0.39;1.38) | 0.27 | 0.964 (0.0020) |
| **Global radial SAX** | **T2** | -1.402 | (-3.62;0.82) | 0.216 | 0.857 (0.032) |
| **Global longitudinal LAX** | **T2** | 0.723 | (0.010;1.44) | 0.047* | 0.689 (0.16) |
| **Global radial LAX** | **T2** | -2.009 | (-4.01;-0.013) | 0.048* | 0.593 (0.29) |
| **Segmental circumferential SAX** | **T2** | 0.366 | (0.018;0.71) | 0.039* | 0.958 (0.0028) |
| **Segmental radial SAX** | **T2** | -0.847 | (-1.62;-0.078) | 0.031* | 0.185 (1.75) |
| **Segmental longitudinal LAX** | **T2** | 0.722 | (0.38;1.07) | <0.001* | 0.864 (0.029) |
| **Segmental radial LAX** | **T2** | -1.923 | (-2.62;-1.23) | <0.001* | 0.775 (0.081) |

## 3.4 Longitudinal association of peak strain recovery and change of relaxation times from baseline to follow-up [model iii)]

Table 10 shows the multi-level mixed-effects regression of myocardial peak strain from baseline to follow-up depending on the change in T1 and T2 relaxation times (ΔT1 and ΔT2). As a longitudinal study, the regression coefficients cover intraindividual variability adjusted for interindividual differences. The regression coefficients quantify the absolute change in myocardial peak strain per 100 ms ΔT1 (T1 time at follow-up minus T1 time at baseline) and 10 ms ΔT2, respectively. The algebraic signs of the regression coefficients and delta relaxation times determine the change in myocardial peak strain. In the case of circumferential strain, a positive ΔT and a positive regression coefficient are linked to a lower absolute peak strain value at follow-up and vice versa (cf. Chapter 1.3).

We found significant associations between decreasing T1 relaxation time and increasing absolute myocardial peak strain from baseline to follow-up in global radial SAX peak strain and all segmental peak strain models. The absolute change in peak strain per 100 ms ΔT1 ranged from 0% (global longitudinal LAX peak strain) to 2.3% (global radial SAX peak strain; numbers are absolute changes; hence, percent is considered a unit). Decreasing T2 relaxation times were significantly related to improving global longitudinal LAX peak strain and segmental radial LAX peak strain from baseline to follow-up. The absolute change in peak strain per 10 ms ΔT2 ranged from 0.1% (global circumferential SAX and segmental circumferential SAX peak strains) to 2.1% (global radial LAX peak strain). The EMB result did not significantly modify the effect of ΔT on peak strain recovery (cf. Table 10 LR test for interaction of ΔT and EMB result).

The 3D margins-plot (Figure 8) shows the marginal (predicted) relations between baseline T1 time, ΔT1, and segmental radial SAX peak strain exemplarily.

**Table 10. Longitudinal association of peak strain recovery and change of relaxation times from baseline to follow-up [model iii)]**

* p < 0.05 indicates statistical significance. ✝ LR test for inclusion of ΔT. ‡ LR test for interaction of ΔT and EMB result. Reg. coef. are adjusted for interindividual differences in strain and T1 and T2 times, myocardial segments (in models with segmental strain), and EMB results (myocarditis or no myocarditis). Applied scaling factors: 100 for T1, 10 for T2. Units are given in square brackets.

CI = confidence interval, EMB = endomyocardial biopsy, LAX = long axes, LR test = likelihood ratio test, Reg. coef. = regression coefficient, SAX = short axis, ΔT = difference of the respective relaxation time at follow-up minus baseline

| | | ΔT [ms] | | | |
|---|---|---|---|---|---|
| **Myocardial peak strain [%]** | | **Reg. coef.** | **95% CI** | **LR test: p ($\chi^2$) †** | **LR test ΔT x EMB: p ($\chi^2$) ‡** |
| **Global circumferential SAX** | **T1** | 0.538 | (-0.25;1.33) | 0.185 (1.76) | 0.772 (0.084) |
| **Global radial SAX** | **T1** | -2.291 | (-4.28;-0.30) | 0.026* (4.94) | 0.769 (0.086) |
| **Global longitudinal LAX** | **T1** | 0.00135 | (-0.45;0.46) | 0.995 (0.00003) | 0.804 (0.062) |
| **Global radial LAX** | **T1** | -0.953 | (-2.27;0.36) | 0.157 (2.00) | 0.860 (0.031) |
| **Segmental circumferential SAX** | **T1** | 0.438 | (0.083;0.79) | 0.016* (5.83) | 0.453 (0.56) |
| **Segmental radial SAX** | **T1** | -1.768 | (-2.53;-1.01) | <0.001* (20.5) | 0.475 (0.51) |
| **Segmental longitudinal LAX** | **T1** | 0.33 | (0.065;0.60) | 0.015* (5.95) | 0.573 (0.32) |
| **Segmental radial LAX** | **T1** | -0.809 | (-1.33;-0.29) | 0.002* (9.18) | 0.785 (0.075) |
| **Global circumferential SAX** | **T2** | 0.0757 | (-0.86;1.02) | 0.875 (0.025) | 0.836 (0.043) |
| **Global radial SAX** | **T2** | -0.398 | (-2.75;1.95) | 0.740 (0.11) | 0.713 (0.14) |
| **Global longitudinal LAX** | **T2** | 0.9 | (0.0041;1.80) | 0.050* (3.85) | 0.903 (0.015) |
| **Global radial LAX** | **T2** | -2.089 | (-4.70;0.52) | 0.118 (2.45) | 0.535 (0.39) |
| **Segmental circumferential SAX** | **T2** | 0.0667 | (-0.31;0.44) | 0.726 (0.12) | 0.661 (0.19) |
| **Segmental radial SAX** | **T2** | -0.253 | (-1.07;0.56) | 0.544 (0.37) | 0.229 (1.44) |
| **Segmental longitudinal LAX** | **T2** | 0.253 | (-0.18;0.68) | 0.249 (1.33) | 0.784 (0.075) |
| **Segmental radial LAX** | **T2** | -1.079 | (-1.93;-0.23) | 0.013* (6.18) | 0.816 (0.054) |

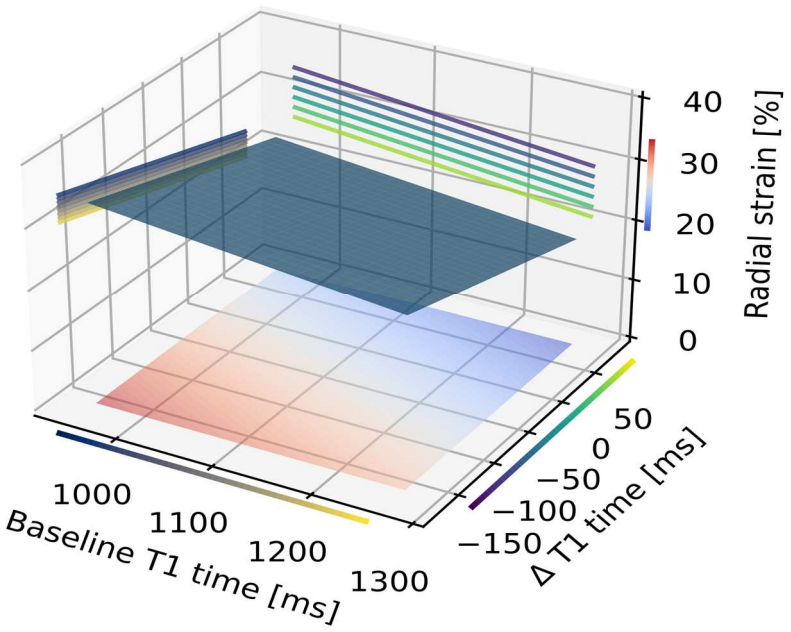


**Figure 8. 3D margins-plot of the multi-level mixed linear regression model for the effect of baseline T1 time and ΔT1 on segmental radial peak strain in SAX view**

The predicted margins for the 5th to the 95th percentile of baseline T1 time (x-axis) and ΔT1 (y-axis) are plotted where all other variables are fixed at their reference level for binary variables and at their mean for continuous variables, respectively. Units are given in square brackets. The dark blue inclined plane describes the effects of baseline T1 time and ΔT1 on the radial peak strain (z-axis). In addition, we projected this surface on the planes spanned by the axes. The color mapping is given next to the scale of the respective axis. The lower the baseline T1 time and the more T1 time reduces from baseline to follow-up, the higher the radial peak strain at follow-up. Across the spread of observed data, this effect is more pronounced for ΔT1 compared to baseline T1 time.

SAX = short axis, ΔT1 = T1 time at follow-up minus T1 time at baseline

## 3.5 Association of baseline relaxation times with functional recovery [model iv)]

Table 11 depicts the association of baseline T1 and T2 relaxation times with functional recovery (increasing absolute peak strain) in the follow-up examination (longitudinal study). The regression coefficients quantify the absolute change in myocardial peak strain from baseline to follow-up per 100 or 10 ms difference in baseline T1 or T2 relaxation time, respectively. In our model, the effect of baseline relaxation times on baseline myocardial peak strain is separated from the effect on myocardial peak strain recovery at follow-up. Hence, the predicted myocardial peak strain at follow-up results from the baseline strain and its recovery, where both depend on the respective baseline relaxation time. Considering the actual regression coefficients for circumferential direction, a negative value describes the (marginal) average absolute strain recovery per 100 ms (10ms) difference of the baseline T1 (T2) time (cf. Chapter 1.3). Hence, the higher the baseline T1 or T2 time, the more pronounced the functional recovery.

All peak strain models in the SAX view (except for global radial SAX) showed significant associations between increased baseline T1 relaxation times and a more substantial functional recovery from baseline to follow-up. More specifically, the higher the baseline T1 relaxation time, the larger the circumferential and radial SAX peak strain recovery. The absolute change in peak strain from baseline to follow-up per 100 ms difference in baseline T1 time ranged from 0.1% (segmental longitudinal LAX peak strain) to 2.2% (global radial SAX peak strain; numbers are absolute changes; hence, percent is considered a unit). Baseline T2 relaxation times were significantly related to the change in global longitudinal LAX and segmental radial SAX peak strains only. The absolute change in peak strain from baseline to follow-up per 10 ms difference in baseline T2 time ranged from 0.4% (segmental circumferential SAX and segmental longitudinal LAX peak strains) to 1.8% (global radial SAX peak strain). The EMB result did not significantly modify the effect of baseline relaxation times on peak strain recovery (cf. Table 11 LR test for three-way interaction of follow-up indicator, baseline relaxation time, and EMB result).

The margins-plot (Figure 9) shows the marginal (predicted) relations between baseline T1 time, strain recovery from baseline to follow-up, and segmental radial SAX peak strain exemplarily.

**Table 11. Association of baseline relaxation times with functional recovery [model iv)]**

* p < 0.05 indicates statistical significance. ✝ Wald's test whether the Reg. coef. equals 0. ‡ LR test for three-way interaction of follow-up indicator [i.e., the binary variable indicating whether an observation is from baseline (= 0) or follow-up (= 1)], baseline relaxation time, and EMB result. Reg. coef. are adjusted for interindividual strain differences in baseline examination, baseline T1 and T2 relaxation times, myocardial segments (in models with segmental strain), and EMB results (myocarditis or no myocarditis). Applied scaling factors: 100 for T1, 10 for T2. Units are given in square brackets.

CI = confidence interval, EMB = endomyocardial biopsy, Int. = interaction, LAX = long axes, LR test = likelihood ratio test, Reg. coef. = regression coefficient, SAX = short axis

| | | Int.: follow-up indicator x baseline relaxation time [ms] | | | |
|---|---|---|---|---|---|
| **Myocardial peak strain [%]** | | **Reg. coef.** | **95% CI** | **p-value Wald test ✝** | **LR test: p ($\chi^2$) ‡** |
| **Global circumferential SAX** | **T1** | -1.046 | (-1.91;-0.18) | 0.018* | 0.851 (0.035) |
| **Global radial SAX** | **T1** | 2.193 | (-0.083;4.47) | 0.059 | 0.485 (0.49) |
| **Global longitudinal LAX** | **T1** | -0.173 | (-0.72;0.38) | 0.539 | 0.729 (0.12) |
| **Global radial LAX** | **T1** | 0.986 | (-0.62;2.60) | 0.23 | 0.800 (0.064) |
| **Segmental circumferential SAX** | **T1** | -0.588 | (-0.99;-0.19) | 0.004* | 0.888 (0.020) |
| **Segmental radial SAX** | **T1** | 1.269 | (0.40;2.14) | 0.004* | 0.246 (1.34) |
| **Segmental longitudinal LAX** | **T1** | -0.129 | (-0.46;0.20) | 0.437 | 0.879 (0.023) |
| **Segmental radial LAX** | **T1** | 0.611 | (-0.028;1.25) | 0.061 | 0.549 (0.36) |
| **Global circumferential SAX** | **T2** | -0.606 | (-1.85;0.63) | 0.338 | 0.735 (0.11) |
| **Global radial SAX** | **T2** | 1.827 | (-1.26;4.91) | 0.246 | 0.732 (0.12) |
| **Global longitudinal LAX** | **T2** | -1.311 | (-2.20;-0.42) | 0.004* | 0.496 (0.46) |
| **Global radial LAX** | **T2** | 1.237 | (-1.44;3.91) | 0.364 | 0.600 (0.27) |
| **Segmental circumferential SAX** | **T2** | -0.397 | (-0.93;0.13) | 0.141 | 0.555 (0.35) |
| **Segmental radial SAX** | **T2** | 1.186 | (0.041;2.33) | 0.042* | 0.358 (0.84) |
| **Segmental longitudinal LAX** | **T2** | -0.411 | (-0.92;0.10) | 0.116 | 0.950 (0.0039) |
| **Segmental radial LAX** | **T2** | 0.899 | (-0.11;1.91) | 0.082 | 0.308 (1.04) |

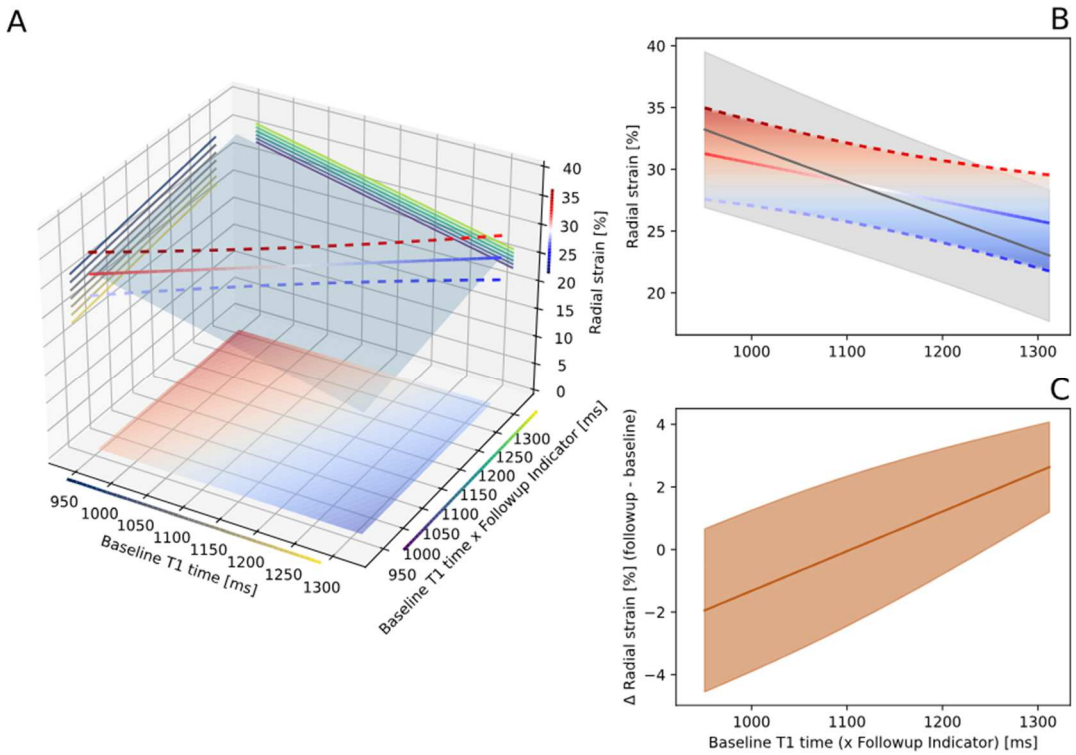


**Figure 9. Margins-plots of the multi-level mixed linear regression model for the effect of baseline T1 time and the effect modification of strain recovery by baseline T1 time**

A: The predicted margins of the segmental radial peak strain in SAX view at follow-up for the 5th to the 95th percentile of baseline T1 time and its interaction with the follow-up indicator [i.e., the binary variable indicating whether an observation is from baseline (= 0) or follow-up (= 1)] are plotted where all other variables are fixed at their reference level for binary variables and at their mean for continuous variables, respectively. Units are given in square brackets. The dark blue inclined plane describes the effects of baseline T1 time (x-axis) and its interaction with the follow-up indicator (y-axis) on the radial peak strain (z-axis). We added a line (with dashed 95% CI) for the predicted strain at follow-up given the (connected) baseline T1. In addition, we projected this surface on the planes spanned by the axes. The color mapping is given next to the scale of the respective axis.

B: The grey line (and 95% CI) describes the marginal effect of the baseline T1 time on the baseline radial strain, and the color-coded line (and its 95% CI) depicts the marginal radial strain at follow-up (equals the line in A) depending on the baseline T1 time.

C: This graph depicts the separated predicted effect of the baseline T1 time on the strain recovery from baseline to follow-up.

The lower the baseline T1 time, the higher the radial peak strain at baseline. In contrast, the higher the baseline T1 time, the higher the recovery of radial strain at follow-up.

CI = confidence interval, SAX = short axis

# 4 Discussion

## 4.1 Key findings

In our study on the functional outcome of patients with suspected myocarditis, we found a significant improvement of myocardial function from the baseline to the follow-up examination. There was a significant association between increased T1 and T2 relaxation times and a lower myocardial peak strain. A decrease in T1 and T2 relaxation times from baseline to follow-up was also significantly related to a recovery of peak strains. Moreover, we found a significant association between an increased baseline T1 relaxation time and a more substantial functional recovery from baseline to follow-up (the higher the baseline T1 time, the more pronounced the strain recovery). Figure 4 gives a graphical overview of our study methods and key results.

Our analyses did not provide evidence for an effect modification by the presence or absence of biopsy-proven myocarditis, indicating that the observed findings are not specific to patients with myocarditis.

## 4.2 Special features of our study

Our study is the first one investigating the relationship between cardiac MRI T1 and T2 relaxation times and myocardial peak strain in patients with clinically suspected myocarditis at the AHA-segmental level. For enhanced accuracy of our results, we benefitted from the EMB-verified diagnosis regarding the presence or absence of myocarditis and the information about temporal evolvement from the baseline to the follow-up examination. For strain analysis through the software platform Segment (Version 3.3 R10187c, Medviso AB, Lund, Sweden, http://segment.heiberg.se) (56), using deformable registration as the underlying FT method, the reproducibility of segmental strain has been demonstrated (33). Moreover, we closely matched cardiac MRI cine sequences and T1 and T2 maps for baseline and follow-up examinations by two mechanisms: AHA-segmentation of the myocardium and transfer of the cine sequences' strain silhouettes onto the maps.

Considering statistical methodology, the traditionally used change score analysis has been shown not to estimate causal effects in observational studies (93). Hence, we applied mixed-effects hierarchical models recommended in this case (63).

The value of myocardial strain has been assessed for various disease entities (64–71) and task fields, e.g., outcome prediction (72–74) and diagnostic assessment (75–77).

Recent publications on myocardial infarction or acute coronary syndrome frequently apply segmental peak strain to measure cardiac function (78–82). In contrast, the approach of AHA-segmental peak strain is a relative novelty in assessing myocardial function in cardiac MRI of patients with myocarditis (83). The majority of recently published studies used LVEF (84–87) or global peak strain (88–93) to quantify myocardial function in myocarditis. However, numerous cardiac diseases do not involve the heart as a whole in the early stages but are limited to regional impairments in separate myocardial segments. Global measures, like the heart's ejection fraction or the global myocardial peak strain, are thus less likely to detect early dysfunction (27–29). Furthermore, strain measurements were intended to serve as a quantitative marker for the regional, not the global, myocardial function in the first place.

## 4.3 Association of positive EMB result with recovery of myocardial peak strain [model i)]

The significant improvement of myocardial function from the baseline to the follow-up examination in our study cohort is not unexpected, ranging from 2.0% (global and segmental circumferential SAX peak strain) to 6.6% (global radial SAX peak strain) during the course of the disease (cf. Table 8). The functional recovery as an expression for the healing process might be traced to physical rest, appropriate medical therapy for heart failure, and/or anti-infective or immunosuppressive medication, respectively.

Literature on the functional outcome, i.e., the development of myocardial function over time, in patients with myocarditis assessed by cardiac MRI is sparse. However, many studies have investigated global and partly regional cardiac function in patients with acute myocarditis one-time. Their two major findings were that a) the myocardial function in patients with myocarditis is significantly lower than in healthy controls, and b) the myocardial strain is more sensitive to detect this impairment than LVEF. These perceptions led the authors to conclude that the myocardial strain could help in diagnosing myocarditis (7,47,71,83,84,88–92,94–100). Currently, functional abnormalities are only regarded as a supportive criterion since they are not specific to myocarditis (23).

In most of the abovementioned studies, echocardiography was used to evaluate LVEF or strain (7,47,71,94,96–100), especially in those with follow-up examinations. This may be due to the fact that echocardiography is less expensive and complex, more widely available, and has fewer contraindications than MRI. In contrast to our investigation, only a few above-cited studies confirmed the suspected diagnosis of myocarditis by EMB,

most likely owing to the risk of complications (7,47). Besides the use of echocardiography instead of MRI and the lack of EMB in resembling myocarditis studies, partly low case numbers, investigations in pediatric patients, or targeting specific diseases, like COVID-19 or systemic lupus erythematosus, make it more difficult to draw comparisons to our work (7,71,83,88,91,94,96–98,100). Surveys that deal with the functional outcome in patients with myocarditis, i.e., that include follow-ups, are less frequent. However, all of those have in common to have found an improvement in cardiac function from baseline to follow-up (7,47,71,89,97,99,100), as we observed, too.

Hypothetically, the observed functional improvement could be based on the “hibernating or stunned myocardium” concept on the cell level. The term “hibernating or stunned myocardium” was initially introduced to describe the reversible state of reduced myocardial contractility due to transient acute ischemia among patients with coronary artery disease. In hibernating or stunned myocardium, the heart muscle cells shut down their contractions to remain viable during ischemia. The difference between hibernating and stunned myocardium is the period it takes the myocardial cells to recover functionally. The myocardial function in hibernating cells can recover as soon as the normal perfusion is restored, e.g., by coronary artery bypass or percutaneous coronary intervention. While hibernating myocardium can return to normal function by the time of reperfusion immediately, stunned myocardium shows persistent wall motion abnormalities for several days despite rapid reperfusion. That means the stunned myocardium has a regular blood supply but is not contractile (101).

This concept could also apply to myocarditis, albeit the underlying tissue damage is not caused by reduced perfusion in the first place as in coronary artery disease. However, regarding the pathomechanism of inflammation, the tissue damage is followed by a short-term ischemic phase, too. Afterward, the ischemia passes into hyperemia and edema. Inflamed myocardial cells might stay viable due to hyperemia as part of the pathophysiological inflammatory process. However, under the impact of a damaging agent, such as microbiological pathogens, toxic substances, or autoimmune reactions, and the resulting immune response, they might not be able to maintain contractions to the same extent as healthy muscle tissue can. After eliminating that damaging agent, hyperemia and edema usually decline, and the surviving myocardial cells might regain their contraction ability. Further investigations could address this hypothesis.

## 4.4 Cross-sectional association of T1 and T2 relaxation times with myocardial peak strain [model ii)]

In our work, we investigated the relationship between myocardial function and myocardial tissue characteristics in myocarditis assessed by cardiac MRI (cf. Table 9). We evaluated the myocardial function via strain values captured from cardiac MRI cine sequences, with lower absolute strain values representing a poorer myocardial function. We used T1 and T2 relaxation times derived from cardiac MRI mapping to quantify myocardial tissue characteristics. Increased free water content in tissues is usually found in expanded extracellular volume and fibrosis, leading to high T1 relaxation times. Thus, T1 mapping can quantify regional or diffuse fibrosis, edema, or amyloidosis, validated by histological findings (102–105). T2 mapping is mainly used to detect myocardial edema, quantified, and reflected by high T2 relaxation times (106,107).

Our cross-sectional analyses show significant associations between increased T1 and T2 relaxation times and lower segmental myocardial peak strain. Partly, such associations apply to global peak strain, too. We conclude that fibrosis and edema in myocardial tissue (quantified by T1 and T2 relaxation times) might cause poor myocardial function in the affected AHA segments, whereby the amounts of fibrosis and edema might be associated with the degree of strain impairment (dose dependency). Pathophysiologically, this finding might be explained by a reduced number of contractile myocardial cells and an increased extracellular volume without contractile ability, filled with edema and fibrosis. In myocarditis, cell damage triggers an immune response, including t-lymphocytes and antibodies, that leads to an inflammatory reaction. The necrotic tissue is removed during that process, and granulation tissue develops, transforming into fibrotic tissue over time (1).

Resembling studies came to the same conclusion (96–98,108). Meindl et al. used LGE in cardiac MRI to detect areas of necrotic, fibrotic, or scarred tissue in 31 patients with myocarditis. They found significantly lower regional longitudinal strain values in AHA segments without LGE, meaning the absolute strain values were higher in segments without LGE. Thus, the myocardial function, assessed by 2D speckle tracking echocardiography, was better in regions without non-ischemic myocardial injury. Similar results have been reported by Kostakou et al. (98). In another study, 33 pediatric myocarditis patients aged between four and 17 years were examined by echocardiography for myocardial strain evaluation and cardiac MRI for fibrosis and edema assessment. The authors demonstrated that the segmental longitudinal strain was significantly impaired in edematous regions in an MRI T2-weighted sequence (97).

Investigating 29 patients with myocarditis, Goody et al. also found significant associations between regional changes in myocardial texture, such as edema, hyperemia, necrosis, and fibrosis [assessed by MRI T2-weighted short tau inversion recovery (STIR) sequences, EGE, and LGE], and reduced segmental longitudinal, radial, and circumferential strain, obtained by 2D and 3D speckle tracking echocardiography (108).

Nevertheless, differences in study design, such as the use of echocardiography instead of cardiac MRI for myocardial strain evaluation and MRI LGE instead of mapping to assess myocardial injury, the lack of EMB to confirm the diagnosis, lower case numbers, and the investigation of pediatric patients or longitudinal strain only, might limit the comparability with our work (96–98,108). To our knowledge, our study is the first to investigate the relationship between segmental myocardial strain derived from cardiac MRI cine sequences and T1 and T2 relaxation times derived from cardiac MRI parametric mapping. Our findings might be of clinical relevance since they suggest that assessing the segmental myocardial strain and the matching T1 and T2 time values allows the localization and evaluation of the extent of myocardial involvement in myocarditis. According to previous studies (27–29,97), the segmental myocardial strain appears to be more sensitive regarding the detection of early and subtle changes in myocarditis compared to conventional echocardiographic parameters like LVEF. As further research might prove, the same could apply to T1 and T2 time values.

## 4.5 Longitudinal association of peak strain recovery and change of relaxation times from baseline to follow-up [model iii)]

Our results show significant associations between decreasing T1 relaxation times and increasing segmental myocardial peak strain values from baseline to follow-up examination (cf. Table 10). For the global strain models, only the radial peak strain's improvement in the SAX view was significantly related to decreasing T1 relaxation times over time. These findings support our hypothesis that regional myocardial function depends on the amount of edema and fibrosis and that functional impairment is at least partially reversible. Thus, a decline, particularly in edema, usually causes an improvement in cardiac function. This assumption has earlier been confirmed by Chinali et al. in their study concerning myocarditis in children. They observed the reversibility of reduced cardiac performance in most patients, too. Moreover, they stated that the presence of fibrosis, depicted by LGE in follow-up cardiac MRI, was significantly higher

in cases with persistently impaired global longitudinal strain in follow-up echocardiography (97).

Several investigations have been conducted to determine the value of T1 mapping in quantifying myocardial fibrosis (104,105). In these studies, EMB was performed to allow the correlation between histology and imaging techniques. The authors discovered significantly lower post-contrast T1 relaxation times in patients with cardiomyopathy or heart failure than in healthy controls. Post-contrast T1 relaxation times were also inversely correlated with histologic fibrosis (104,105). Moreover, the worse the diastolic function, assessed by echocardiography, the shorter the post-contrast T1 relaxation times, as stated by Iles et al. (104). The latter indicates an impairment in diastolic function due to diffuse fibrosis. However, these results can not directly be compared to our findings since we analyzed native cardiac MRI mapping in patients with suspected myocarditis. In contrast, post-contrast T1 mapping was used in patients with cardiomyopathy or heart failure in the abovementioned studies. The MRI contrast agent gadolinium lowers T1 relaxation times, so in fibrotic tissue with lately washed-out gadolinium, T1 relaxation times were shorter than in healthy tissue (104,105). In our investigation, based on native T1 mapping, T1 relaxation times are higher in functionally impaired regions of the myocardium. Nevertheless, the authors of the studies mentioned above conclude that myocardial T1 relaxation times represent diffuse fibrosis (104,105).

In our analyses, decreasing T2 relaxation times from baseline to follow-up were only significantly associated with improving global longitudinal peak strain in LAX and segmental radial peak strain in LAX. As explained earlier, high T2 relaxation times reflect edema in myocardial tissue (106,107). Moreover, some studies suggest increased T1 relaxation times also provide evidence for myocardial edema (e.g., (109)).

The unassisted reversibility of myocardial fibrosis is assumed to be strongly limited (110). Hence, the described decline mainly in edema (quantified by T1 and T2 relaxation times) and the growth in myocardial function are consistent with the typical pathophysiological course of myocarditis, where tissue damage and reduced function are predominantly observed in the acute and subacute phases of the disease (111). On average, follow-up investigations in the MyoRacer-Trial have been conducted three to four months after baseline examination, where myocardial tissue and its functionality usually are about to recover. Thus, cardiac MRI mapping techniques may help assess the degree of inflammation and discriminate between the different stages of the disease. Additionally, repeated application of cardiac MRI mapping can be a valuable tool to monitor the healing process and to indicate a necessary EMB in patients with persistent inflammation

to determine further treatment. The outstanding performance of native T1 and T2 mapping and longitudinal strain in diagnosing myocardial inflammation compared to conventional cardiac MRI parameters (as used in the LLC) has already been confirmed by earlier studies (109,112–114). Moreover, native mapping techniques do not require the application of contrast agents, which is another advantage (114).

## 4.6 Association of baseline relaxation times with functional recovery [model iv)]

Increased T1 and T2 baseline relaxation times were significantly associated with a more substantial strain recovery from baseline to follow-up in our study population (cf. Table 11). I.e., the higher the baseline relaxation time, the larger the functional recovery. This finding suggests that pronounced pathological changes in inflamed myocardial tissue, especially edema (as fibrotic changes usually only appear in late disease stages at FU examinations (2,13,115)), may be reversible, so damaged tissue appears to have a high capacity to recover. We conclude that T1 and T2 relaxation times at baseline can be of prognostic value regarding functional recovery in myocarditis.

Earlier studies obtained similar results, using LVEF to quantify the myocardial function instead of myocardial peak strain, as we did (47,109,116). In a large study including 443 patients with confirmed myocarditis, Ammirati et al. found correlations between complicated myocarditis at baseline (LVEF < 50% on the first in-hospital echocardiogram) and a significantly higher functional recovery in follow-up. The average LVEF improvement in patients with complicated myocarditis from baseline to follow-up amounted to 3%. However, the study suffered a significant loss to follow-up (51.8%) since it was designed retrospectively. Thus, follow-up examinations were only conducted in case of clinical need, perhaps leading to a biased study population in follow-up. Moreover, a histological examination of the myocardium was merely performed in 13.7% of all patients (47). Luetkens et al. reported a significant association between baseline T1 and T2 relaxation times and the difference in LVEF from baseline to follow-up in patients with myocarditis (109). Vermes et al. also found that myocardial edema at baseline was strongly correlated to a rise in LVEF ≧ 5% during the healing process of inflamed myocardium (116).

In our analyses, the absolute functional improvement from baseline to follow-up ranged from 2.0% (global and segmental circumferential SAX peak strain) to 6.6% (global radial SAX peak strain) with significant correlations to baseline T1 relaxation time for global and segmental circumferential and segmental radial peak strain in SAX view. Despite

the use of myocardial peak strain instead of LVEF, our work's underlying trend of associations is consistent with the abovementioned studies (47,109,116).

## 4.7 EMB effect modification

In the MyoRacer-Trial, EMB was performed to confirm or rule out suspected myocarditis. As likelihood ratio tests showed, the EMB result did not exhibit an effect modification for the observed associations. I.e., the correlations between myocardial peak strain and T1 and T2 relaxation times are valid for all MyoRacer probands, regardless of a positive or negative EMB result for myocarditis. Since the observed associations are not specific to biopsy-proven myocarditis in our work, it is conceivable that they might also apply to other cardiological patients presenting with myocardial edema, fibrosis, and impaired LV function to some extent. Consequently, baseline T1 and T2 relaxation times, both quantifying myocardial edema (among other things), might also help predict the development of LV function in further cardiac disease entities involving the myocardial tissue.

In our analyses, one exception showed up for the cross-sectional association between segmental radial peak strain in LAX and T1 relaxation time (cf. Table 9). We obtained a significant effect modification by EMB result for this particular statistical model, likely caused by multiple testing without correction. Moreover, myocarditis in EMB was significantly associated with lower segmental radial peak strain in the SAX view in the baseline examination (cf. Table 8). I.e., on average, patients with an EMB-confirmed diagnosis of myocarditis had a worse LV function at baseline than EMB-negative patients. Although this correlation applied to segmental radial peak strain in SAX view only, it is comprehensible due to the early pathological changes in inflamed myocardial tissue, such as edema. As explained above, our analyses linked these changes to impaired myocardial function.

All things considered, the observed associations between myocardial strain and T1 and T2 relaxation times could possibly apply to patients with various myocardial disease entities. This presumption appears coherent, even if no resembling studies can serve as references yet. Thus, it could be a target for future research.

## 4.8 Segmental versus global peak strain models

The myocardial strain serves as a quantitative marker for the regional function of the myocardium. Numerous cardiac diseases do not involve the heart as a whole in the early

stages but are limited to regional impairments in separate myocardial segments. Global measures, like the heart's ejection fraction, are thus less likely to catch early dysfunction (27–29). Various studies confirmed that global myocardial strain values were superior to LVEF regarding the early identification of LV dysfunction and the prediction of the development of major adverse cardiovascular events (74,77,93,98).

For our work's investigated correlations between myocardial strain and T1 and T2 relaxation times, segmental peak strain models showed more often significant p-values than global peak strain models, indicating that the segmental strain might be more accurate, especially concerning the extent and localization of myocardial damage. Among the segmental models, the radial peak strain was the only one with significant associations for all analyzed combinations in our study. Literature on the value of segmental myocardial peak strain regarding the diagnosis and prognosis of myocarditis needs to be more extensive. However, some studies have investigated segmental longitudinal strain (96,97,108), observing a significant concordance between myocardial segments with impaired longitudinal strain and regional changes in texture. Our results suggest that the segmental radial peak strain might be even more reliable than the segmental longitudinal peak strain, especially regarding the prediction of functional development depending on the baseline T1 and T2 relaxation times. Thus, a regular survey of segmental myocardial peak strain parameters in the setting of clinically suspected myocarditis can be recommended.

## 4.9 Clinical implications

Regarding pathophysiological processes in typical myocarditis, damage to cardiomyocytes is based on the toxic agent, the body’s immune response to it, and potentially resulting autoimmune reactions. The disease can become chronic if pathogens are not entirely eliminated or the immune response does not stop (13). Pathological changes in the inflamed myocardium often include the development of fibrosis caused by increased collagen anabolism. This condition can be partially reversible but can also become permanent. The latter is known as myocardial remodeling, leading to stiffer and tighter heart walls and, thus, to systolic and diastolic dysfunction. It is long-term linked to DCM and heart failure (115).

Our analyses revealed that the higher the baseline T1 relaxation time (quantifying myocardial edema and regional or diffuse fibrosis (102–105)), the larger the recovery of myocardial strain at follow-up. Hence, identifying myocarditis activity on the segmental level may be a treatment target for (potentially MRI-guided) intramyocardial injections of

stem cells for patients with an incomplete or scarcely proceeding fibrosis regression during the healing process. The therapeutic injection of stem cells directly into the myocardium after cardiac ischemia has been a research subject in recent decades (115,117–123). The stem cells often derive from abdominal adipose tissue (adipose-derived stromal cells, ASC) or the bone marrow (mesenchymal stromal cells, MSC) (124). Several preclinical trials have been conducted in animals to investigate the potential of MSC injections in infarcted hearts. Promising results were observed, such as decreased scar tissue and improved contractility (125–128). Hence, research has been continued by clinical trials of MSC therapy for cardiac repair in patients with acute myocardial infarction and chronic ischemic cardiomyopathy. In various studies, patients with ischemic heart failure with reduced ejection fraction (HFrEF) benefitted from intramyocardial injections of autologous ASC or MSC, e.g., reflected by improved cardiac function (LVEF), reduced scar tissue, and fewer hospitalizations due to angina pectoris attacks after four years (124,129,130). Moreover, the results of the POSEIDON-DCM (Percutaneous Stem Cell Injection Delivery Effects on Neomyogenesis in Dilated Cardiomyopathy) study demonstrated an improvement in myocardial function and quality of life in patients with DCM treated with MSC (131,132).

The positive effects of MSC on diseased myocardium primarily comprise an immune response suppression and a paracrine release of stimulating and trophic messenger substances that support the resident cells in repairing the damaged tissue. The differentiation of stem cells to heart muscle cells only plays a tangential role in regeneration (117,133,134). Treatment with stem cell injections in pathologically changed heart tissue might help prevent or regenerate myocardial remodeling and its consequences, such as DCM and heart failure. Our results suggest that regional T1 and T2 relaxation times and myocardial strain are valuable tools for identifying myocardial segments affected by fibrosis, edema, and functional impairment in patients with clinically suspected myocarditis. Those segments could serve as targets for intramyocardial stem cell therapy, too.

Moreover, our analyses show strong correlations between myocardial function and tissue characteristics, regardless of the EMB result. Thus, an early comprehensive cardiac MRI for patients with clinically suspected myocarditis appears valuable for detecting even subtle pathological changes and making a quick diagnosis so that an EMB might not be necessary. The depiction of regional MRI strain values and relaxation times of the whole LV myocardium (in contrast to a few separate samples from EMB) also provides more

detailed information on the localization of affected myocardial tissue and the extent of myocardial injury in these areas.

## 4.10 Study limitations

Several limitations of this study merit consideration. First, as with all non-experimental observational studies, the ability to conclude causal effects from the data is limited, and the results should be interpreted as hypothesis-generating. In our study, the dose-dependent effect of myocardial relaxation times on cardiac function in cross-sectional and longitudinal contexts is highly suggestive of a causal relation or, at least, that we observe strong proxies of these effects.

Second, this secondary analysis of a non-randomized diagnostic trial study was not *a priori* specified. Hence, the power necessary to test the investigated hypothesis was not considered in the original study design and inclusion of patients. Also, multiple comparisons conducted in this study will likely inflate Type-1-Error. Moreover, we did not apply any correction for multiple comparisons due to the non-experimental design of our study (62).

Third, we performed a complete case analysis without imputation of missing data, which may lead to biased estimates of the investigated associations. Both, the computational complexity and the complexity in the specification of the missingness model in multilevel hierarchical data, impeded the use of adequate imputation methods in this study.

Fourth, measuring T1 and T2 time is challenging (135) and is prone to various error sources (acquisition, coregistration, exponential fitting, segmentation). This uncertainty on the predictor variables may have caused regression-dilution bias with consequently shrunken absolute regression coefficients. Therefore, weak associations may have been masked in our statistical analysis. However, we tried to limit these effects by an iterative registration procedure and the applied weighting and masking of the regions of interest to measure segmental relaxation times by the residuals ($r^2$) of the model fitting procedure.

Fifth, the acquired MRI mapping and cine sequences used in this study do not cover all segments of the AHA model of the LV myocardium since no 3-chamber views had been obtained. Also, for the apical and basal layers in the SAX view, no T1 or T2 maps were available. Thus, our results concerning the relations between strain and T1 and T2 relaxation times refer to the LV in the 2Ch view, 4Ch view, and the midventricular layer of the SAX view only. Hence, the term “global” peak strain may be misleading. Moreover,

myocardial tissue characteristics of the RV could not be depicted in cardiac MRI mapping since the myocardium layer is generally too thin.

Further, this work only followed up with the in-plane association of relaxation time and segmental peak strain. The relation of T1 time and perpendicular strain (e.g., the relation between longitudinal strain from the 4Ch plane and 2Ch plane with relaxation times from corresponding SAX segments) could be addressed in further studies, preferably with a cardiac MRI sequence protocol covering all AHA segments. Also, emerging three-dimensional imaging techniques for cine (136) or mapping sequences (137,138) could allow the investigation on an even more granular and comprehensive level.

Finally, measuring segmental peak strain values via speckle tracking is demanding since regional tissue patterns usually do not offer notable landmarks to be tracked. In contrast, for global strain assessment, the heart's apex and the mitral annulus serve as solid and relatively constant landmarks during the cardiac cycle. Thus, interobserver variability has been reported to be higher than for evaluating global peak strain (139).

## 4.11 Conclusion

Our cross-sectional and longitudinal analyses provide evidence of dose-dependent correlations between T1 and T2 relaxation times and myocardial peak strain in patients with clinical presentation of myocarditis, regardless of the EMB result. Thus, assessing strain values and mapping relaxation times helps estimate the functional prognosis in patients with clinically suspected myocarditis.

Due to the strong correlations between myocardial function and tissue characteristics on the segmental level in our analyses, an early comprehensive cardiac MRI for patients with clinically suspected myocarditis appears valuable for detecting subtle pathological changes and making a quick diagnosis. The regional values of strain and relaxation times also provide detailed information on the localization of affected myocardial tissue and the extent of myocardial injury in these areas. The segmental myocardial strain appears to be more sensitive regarding the detection of early and subtle changes in myocarditis compared to conventional echocardiographic parameters like LVEF. More precisely, our results suggest that the segmental radial peak strain might be even more reliable than the segmental longitudinal peak strain, especially regarding the prediction of functional development depending on the baseline T1 and T2 relaxation times.

Moreover, cardiac MRI repetitions, including segmental peak strain evaluation and T1 and T2 mapping, help monitor the inflammation activity and the healing process during the course of the disease. Thus, patients in need for specific therapies or further

diagnostic investigations, such as EMB, can be recognized. Finally, our results might also apply to other myocardial disease entities since we did not find an effect modification by the presence of myocarditis in EMB.

## 4.12 Outlook

To estimate the development of the LV function during the healing process of myocardial inflammation is fundamental for planning follow-up examinations and deciding treatment options. So eligible parameters for making reliable predictions on the functional outcome must be explored further. In this regard, a viable approach could be the combination of T1 and T2 relaxation times. Moreover, surveys on alternative outcomes in patients with myocarditis, e.g., concerning the quality of life or the New York Heart Association (NYHA) status in the follow-up investigation, enrich future research content with data derived from the MyoRacer-Trial.

The early diagnosis of myocarditis via subtle changes in myocardial tissue, represented by T1 and T2 time values in cardiac MRI mapping, could also be subject to further investigation. As for segmental myocardial strain, the sensitivity of these variables regarding the early detection of inflammation might be higher than that of conventional echocardiographic parameters like LVEF.

The associations between myocardial strain and T1 and T2 relaxation times observed in this work may apply to patients with various myocardial disease entities. Since no resembling studies are available to reference, this could be another target for future research. Further, the present investigation only followed up with the in-plane association of relaxation times and segmental peak strain. The relation of T1 time and perpendicular strain (e.g., the relation between longitudinal strain from the 4Ch plane and 2Ch plane with relaxation times from corresponding SAX segments) could be addressed in further studies, preferably with a cardiac MRI sequence protocol covering all AHA segments. Also, emerging three-dimensional imaging techniques for cine (136) or mapping sequences (137,138) could allow the investigation on an even more granular and comprehensive level.

# 5 Summary

## 5.1 Summary

The relation between LV function and cardiac MRI tissue characteristics in separate myocardial segments and their change over time has yet to be explored in myocarditis. Thus, our research aimed to investigate possible associations between global and regional myocardial T1 and T2 times and peak strain in patients with suspected myocarditis.

From 2012 to 2015, 129 patients with clinically suspected myocarditis of the prospective, observational MyoRacer-Trial underwent systematic biventricular EMB at baseline and cardiac MRI at baseline and after three months as a follow-up. We divided the LV myocardium into 17 segments and estimated the segmental myocardial strain using FT. We registered T1 and T2 maps to the cine sequences and transferred the segmentations used for FT to ensure conformity of the myocardial segments. Multi-level multivariable linear mixed effects regression was applied to investigate the relation of segmental myocardial strain to relaxation times and their respective change from baseline to follow-up.

We found a significant improvement in myocardial peak strain from baseline to follow-up ($p < 0.001$; all p-values given for likelihood ratio tests) and significant associations between higher T1 and T2 times and lower segmental myocardial peak strain (p ranging from < 0.001 to 0.049). E.g., regression coefficient (Reg. coef.) for segmental radial peak strain in short axis view (SRPS_SAX) and T1 time: -1.9, 95% CI (-2.6;-1.2) %/100 ms, $p < 0.001$. A decrease in T1 and T2 times from baseline to follow-up was also significantly related to a recovery of segmental peak strains (p ranging from < 0.001 to 0.050). E.g., Reg. coef. for SRPS_SAX per ΔT1: -1.8, 95% CI (-2.5;-1.0) %/100 ms, $p < 0.001$. Moreover, the higher the baseline T1 time, the more substantial the functional recovery from baseline to follow-up (p ranging from 0.004 to 0.042, e.g., for SRPS_SAX: Reg. coef. 1.3, 95% CI (0.4;2.1) %/100 ms, p 0.004). We did not find an effect modification by the presence of myocarditis in the EMB ($p > 0.1$).

Our cross-sectional and longitudinal analyses provide evidence of dose-dependent correlations between T1 and T2 relaxation times and myocardial peak strain in patients with clinical presentation of myocarditis, regardless of the EMB result. Thus, assessing strain values and mapping relaxation times helps estimate the functional prognosis in patients with clinically suspected myocarditis.

## 5.2 Zusammenfassung

Die Zusammenhänge zwischen der kardialen linksventrikulären (LV) Funktion und magnetresonanztomographisch erhebbaren Parametern des Myokards sowie deren jeweiligen Entwicklungen im zeitlichen Verlauf einer Myokarditis sind bisher nicht umfassend untersucht. Daher beschäftigt sich die vorliegende Arbeit mit der Erforschung des Verhältnisses von globalen und regionalen peak strain-Werten und T1 und T2 Zeiten des LV Myokards in der Magnetresonanztomographie (MRT) bei Patienten mit Verdacht auf Myokarditis.

Die MyoRacer-Studie ist eine prospektive Beobachtungsstudie, die von 2012 bis 2015 am Herzzentrum des Universitätsklinikums Leipzig durchgeführt wurde. Dabei wurden 129 Patienten mit klinischem Verdacht auf Myokarditis mittels biventrikulärer Myokardbiopsie sowie kardialer MRT untersucht. Drei Monate nach der Erstuntersuchung (EU) erfolgte eine MRT-Folgeuntersuchung (FU). Für unsere Analysen unterteilten wir das LV Myokard standardmäßig in 17 Segmente, um mithilfe der Technik des feature trackings den segmentalen peak strain zu evaluieren. Weiterhin registrierten wir T1 und T2 maps gegen cine-Sequenzen der MRT und übertrugen die Segmentierungen aus den cine-Sequenzen zwecks Übereinstimmung in die MRT maps. Anschließend analysierten wir die Zusammenhänge zwischen segmentalem strain und T1 und T2 Zeiten und deren jeweiligen Veränderungen im zeitlichen Verlauf mithilfe eines hierarchischen, multivariablen, gemischten linearen Regressionsmodells.

Unsere Ergebnisse zeigen eine signifikante Verbesserung der peak strain-Werte von der EU zur FU ($p < 0.001$; alle p-Werte für likelihood ratio tests angegeben) sowie eine signifikante Assoziation von erhöhten T1 und T2 Zeiten mit verminderten segmentalen peak strain-Werten (p zwischen < 0.001 und 0.049). Weiterhin war ein Abfall der T1 und T2 Zeiten von der EU zur FU signifikant mit einer Erholung der segmentalen peak strain-Werte verknüpft (p zwischen < 0.001 und 0.050). Je höher die T1 Zeiten bei der EU ausfielen, desto stärker erholte bzw. verbesserte sich der peak strain von der EU zur FU (p zwischen 0.004 und 0.042). Eine Effektmodifikation durch den bioptischen Nachweis einer Myokarditis war nicht zu beobachten ($p > 0.1$).

Unsere Quer- und Längsschnittanalysen belegen dosisabhängige Zusammenhänge zwischen T1 und T2 Zeiten und myokardialen peak strain-Werten bei Patienten mit dem klinischen Bild einer Myokarditis, unabhängig vom Ergebnis der Myokardbiopsie. Daher ist die Bestimmung von T1 und T2 Zeiten und myokardialem strain mittels kardialer MRT zur Abschätzung der funktionellen Prognose bei Patienten mit klinischem Verdacht auf Myokarditis hilfreich.

# 6 References


1. Leone O, Pieroni M, Rapezzi C, Olivotto I. The spectrum of myocarditis: from pathology to the clinics. Virchows Arch. 2019;475(3):279–301.

2. Lampejo T, Durkin SM, Bhatt N, Guttmann O. Acute myocarditis: aetiology, diagnosis and management. Clin Med . 2021;21(5):e505–e510.

3. Dai H, Lotan D, Much AA, et al. Global, Regional, and National Burden of Myocarditis and Cardiomyopathy, 1990-2017. Front Cardiovasc Med. 2021;8:610989.

4. Leuschner F, Katus HA, Kaya Z. Autoimmune myocarditis: past, present and future. J Autoimmun. Elsevier BV; 2009;33(3-4):282–289.

5. Baessler B, Luecke C, Lurz J, et al. Cardiac MRI and Texture Analysis of Myocardial T1 and T2 Maps in Myocarditis with Acute versus Chronic Symptoms of Heart Failure. Radiology. 2019;292(3):608–617.

6. Fung G, Luo H, Qiu Y, Yang D, McManus B. Myocarditis. Circ Res. 2016;118(3):496–514.

7. Ammirati E, Lupi L, Palazzini M, et al. Prevalence, Characteristics, and Outcomes of COVID-19-Associated Acute Myocarditis. Circulation. 2022;145(15):1123–1139.

8. Ammirati E, Moslehi JJ. Diagnosis and Treatment of Acute Myocarditis: A Review. JAMA. 2023;329(13):1098–1113.

9. Kindermann I, Ukena C, Mahfoud F, Böhm M, Yilmaz A, Klingel K. Myokarditis-Update. Der Kardiologe. 2016;10(5):311–330.

10. Shah MD, Sumeh AS, Sheraz M, Kavitha MS, Venmathi Maran BA, Rodrigues KF. A mini-review on the impact of COVID 19 on vital organs. Biomed Pharmacother. 2021;143:112158.

11. Kawakami R, Sakamoto A, Kawai K, et al. Pathological Evidence for SARS-CoV-2 as a Cause of Myocarditis: JACC Review Topic of the Week. J Am Coll Cardiol. 2021;77(3):314–325.

12. Zepp F, Knuf M. „Coronavirus disease 2019 (COVID-19)“ im Kindes- und

Jugendalter. Monatsschr Kinderheilkd. 2021;169(11):1010–1033.

13. Heymans S, Eriksson U, Lehtonen J, Cooper LT Jr. The Quest for New Approaches in Myocarditis and Inflammatory Cardiomyopathy. J Am Coll Cardiol. 2016;68(21):2348–2364.

14. Caforio ALP, Pankuweit S, Arbustini E, et al. Current state of knowledge on aetiology, diagnosis, management, and therapy of myocarditis: a position statement of the European Society of Cardiology Working Group on Myocardial and Pericardial Diseases. Eur Heart J. 2013;34(33):2636–2648, 2648a – 2648d.

15. Rroku A, Kottwitz J, Heidecker B. Update on myocarditis - what we know so far and where we may be heading. Eur Heart J Acute Cardiovasc Care. 2020; doi: 10.1177/2048872620910109.

16. Writing Committee, Gluckman TJ, Bhave NM, et al. 2022 ACC expert consensus decision pathway on cardiovascular sequelae of COVID-19 in adults: Myocarditis and other myocardial involvement, post-acute sequelae of SARS-CoV-2 infection, and return to play: A report of the American college of cardiology solution set oversight committee. J Am Coll Cardiol. Elsevier BV; 2022;79(17):1717–1756.

17. Francone M, Chimenti C, Galea N, et al. CMR sensitivity varies with clinical presentation and extent of cell necrosis in biopsy-proven acute myocarditis. JACC Cardiovasc Imaging. 2014;7(3):254–263.

18. Greulich S, Seitz A, Müller KAL, et al. Predictors of Mortality in Patients With Biopsy-Proven Viral Myocarditis: 10-Year Outcome Data. J Am Heart Assoc. 2020;9(16):e015351.

19. Baessler B, Luecke C, Lurz J, et al. Cardiac MRI Texture Analysis of T1 and T2 Maps in Patients with Infarctlike Acute Myocarditis. Radiology. Radiological Society of North America; 2018;289(2):357–365.

20. Caforio ALP, Calabrese F, Angelini A, et al. A prospective study of biopsy-proven myocarditis: prognostic relevance of clinical and aetiopathogenetic features at diagnosis. Eur Heart J. 2007;28(11):1326–1333.

21. Kindermann I, Kindermann M, Kandolf R, et al. Predictors of outcome in patients with suspected myocarditis. Circulation. 2008;118(6):639–648.

22. Yilmaz A, Kindermann I, Kindermann M, et al. Comparative Evaluation of Left and Right Ventricular Endomyocardial Biopsy. Circulation. 2010. p. 900–909. doi: 10.1161/circulationaha.109.924167.

23. Ferreira VM, Schulz-Menger J, Holmvang G, et al. Cardiovascular Magnetic Resonance in Nonischemic Myocardial Inflammation: Expert Recommendations. J Am Coll Cardiol. 2018;72(24):3158–3176.

24. Bloch F. Nuclear Induction. Phys Rev. American Physical Society; 1946;70(7-8):460–474.

25. MRI Questions & Answers; MR imaging physics & technology. Questions and Answers in MRI. https://mriquestions.com/index.html. Accessed December 16, 2022.

26. Friedrich MG, Sechtem U, Schulz-Menger J, et al. Cardiovascular magnetic resonance in myocarditis: A JACC White Paper. J Am Coll Cardiol. 2009;53(17):1475–1487.

27. Almutairi HM, Boubertakh R, Miquel ME, Petersen SE. Myocardial deformation assessment using cardiovascular magnetic resonance-feature tracking technique. Br J Radiol. 2017;90(1080):20170072.

28. Lorca MCN, Haraldsson H, Ordovas KG. Ventricular mechanics: techniques and applications. Magn Reson Imaging Clin N Am. 2015;23(1):7–13.

29. Scatteia A, Silverio A, Padalino R, et al. Non-Invasive Assessment of Left Ventricle Ejection Fraction: Where Do We Stand? J Pers Med. 2021;11(11). doi: 10.3390/jpm11111153.

30. Ridgway JP. Cardiovascular magnetic resonance physics for clinicians: part I. J Cardiovasc Magn Reson. 2010;12(1):71.

31. Moghari MH, Barthur A, Amaral ME, Geva T, Powell AJ. Free-breathing whole-heart 3D cine magnetic resonance imaging with prospective respiratory motion compensation. Magn Reson Med. 2018;80(1):181–189.

32. Fischer K, Obrist SJ, Erne SA, et al. Feature Tracking Myocardial Strain Incrementally Improves Prognostication in Myocarditis Beyond Traditional CMR

Imaging Features. JACC Cardiovasc Imaging. 2020;13(9):1891–1901.

33. Dobrovie M, Barreiro-Pérez M, Curione D, et al. Inter-vendor reproducibility and accuracy of segmental left ventricular strain measurements using CMR feature tracking. Eur Radiol. 2019;29(12):6846–6857.

34. Mirsky I, Parmley WW. Assessment of passive elastic stiffness for isolated heart muscle and the intact heart. Circ Res. 1973;33(2):233–243.

35. McCormick M. N-Dimensional Computation of Strain Tensor Images in the Insight Toolkit. Insight J. 2017;2017. doi: 10.54294/1wtpo8.

36. Ferreira VM, Piechnik SK, Dall'Armellina E, et al. T(1) mapping for the diagnosis of acute myocarditis using CMR: comparison to T2-weighted and late gadolinium enhanced imaging. JACC Cardiovasc Imaging. 2013;6(10):1048–1058.

37. Thavendiranathan P, Walls M, Giri S, et al. Improved detection of myocardial involvement in acute inflammatory cardiomyopathies using T2 mapping. Circ Cardiovasc Imaging. 2012;5(1):102–110.

38. Busse A, Rajagopal R, Yücel S, et al. Cardiac MRI-Update 2020. Radiologe. 2020;60(Suppl 1):33–40.

39. Mordi I, Bezerra H, Carrick D, Tzemos N. The Combined Incremental Prognostic Value of LVEF, Late Gadolinium Enhancement, and Global Circumferential Strain Assessed by CMR. JACC Cardiovasc Imaging. 2015;8(5):540–549.

40. Grün S, Schumm J, Greulich S, et al. Long-term follow-up of biopsy-proven viral myocarditis: predictors of mortality and incomplete recovery. J Am Coll Cardiol. 2012;59(18):1604–1615.

41. Anzini M, Merlo M, Sabbadini G, et al. Long-term evolution and prognostic stratification of biopsy-proven active myocarditis. Circulation. 2013;128(22):2384–2394.

42. Cerqueira MD, Weissman NJ, Dilsizian V, et al. Standardized myocardial segmentation and nomenclature for tomographic imaging of the heart. A statement for healthcare professionals from the Cardiac Imaging Committee of the Council on Clinical Cardiology of the American Heart Association. Circulation.

2002;105(4):539–542.

43. Kotanidis CP, Bazmpani M-A, Haidich A-B, Karvounis C, Antoniades C, Karamitsos TD. Diagnostic Accuracy of Cardiovascular Magnetic Resonance in Acute Myocarditis: A Systematic Review and Meta-Analysis. JACC Cardiovasc Imaging. 2018;11(11):1583–1590.

44. Lagan J, Schmitt M, Miller CA. Clinical applications of multi-parametric CMR in myocarditis and systemic inflammatory diseases. Int J Cardiovasc Imaging. 2018;34(1):35–54.

45. Lurz P, Luecke C, Eitel I, et al. Comprehensive Cardiac Magnetic Resonance Imaging in Patients With Suspected Myocarditis: The MyoRacer-Trial. J Am Coll Cardiol. 2016;67(15):1800–1811.

46. Kühn B, Shapiro ED, Walls TA, Friedman AH. Predictors of outcome of myocarditis. Pediatr Cardiol. 2004;25(4):379–384.

47. Ammirati E, Cipriani M, Moro C, et al. Clinical Presentation and Outcome in a Contemporary Cohort of Patients With Acute Myocarditis: Multicenter Lombardy Registry. Circulation. 2018;138(11):1088–1099.

48. Iqbal SUR, Tipoo Sultan FA. Clinical features, cardiac magnetic resonance imaging findings and outcome of patients with suspected myocarditis. J Pak Med Assoc. 2021;71(10):2454–2456.

49. Tschöpe C, Ammirati E, Bozkurt B, et al. Myocarditis and inflammatory cardiomyopathy: current evidence and future directions. Nat Rev Cardiol. 2021;18(3):169–193.

50. Magnetic Resonance Imaging in Myocarditis - Full Text View - ClinicalTrials.Gov. . https://clinicaltrials.gov/ct2/show/NCT02177630. Accessed December 3, 2022.

51. Laqua FC, Amar H, Piotr W, et al. A scalable open-source parallelized python framework for calculating cardiac T1 and T2 maps using Tensorflow on CPU and GPU. .

52. Delso G, Farré L, Ortiz-Pérez JT, et al. Improving the robustness of MOLLI T1 maps with a dedicated motion correction algorithm. Sci Rep. 2021;11(1):18546.

53. Avants BB, Epstein CL, Grossman M, Gee JC. Symmetric diffeomorphic image registration with cross-correlation: evaluating automated labeling of elderly and neurodegenerative brain. Med Image Anal. 2008;12(1):26–41.

54. Tustison NJ, Cook PA, Klein A, et al. Large-scale evaluation of ANTs and FreeSurfer cortical thickness measurements. Neuroimage. 2014;99:166–179.

55. O'Brien AT, Gil KE, Varghese J, Simonetti OP, Zareba KM. T2 mapping in myocardial disease: a comprehensive review. J Cardiovasc Magn Reson. 2022;24(1):33.

56. Heiberg E, Sjögren J, Ugander M, Carlsson M, Engblom H, Arheden H. Design and validation of Segment--freely available software for cardiovascular image analysis. BMC Med Imaging. 2010;10:1.

57. Berggren K, Hedström E, Ehrenborg KS, et al. Multiple Convolutional Neural Networks for Robust Myocardial Segmentation. Svenska Sällskapet för Automatiserad Bildanalys, Helsingborg. 2020; http://medviso.com/documents/BerggrenSSBA2020.pdf.

58. Heyde B, Jasaityte R, Barbosa D, et al. Elastic image registration versus speckle tracking for 2-D myocardial motion estimation: a direct comparison in vivo. IEEE Trans Med Imaging. 2013;32(2):449–459.

59. Morais P, Marchi A, Bogaert JA, et al. Cardiovascular magnetic resonance myocardial feature tracking using a non-rigid, elastic image registration algorithm: assessment of variability in a real-life clinical setting. J Cardiovasc Magn Reson. 2017;19(1):24.

60. Fedorov A, Beichel R, Kalpathy-Cramer J, et al. 3D Slicer as an image computing platform for the Quantitative Imaging Network. Magn Reson Imaging. 2012;30(9):1323–1341.

61. Yaniv Z, Lowekamp BC, Johnson HJ, Beare R. SimpleITK Image-Analysis Notebooks: a Collaborative Environment for Education and Reproducible Research. J Digit Imaging. 2018;31(3):290–303.

62. Rothman KJ. No adjustments are needed for multiple comparisons. Epidemiology. 1990;1(1):43–46.

63. Tennant PWG, Arnold KF, Ellison GTH, Gilthorpe MS. Analyses of “change scores” do not estimate causal effects in observational data. Int J Epidemiol. 2022;51(5):1604–1615.

64. Heydari B, Satriano A, Jerosch-Herold M, et al. 3-Dimensional Strain Analysis of Hypertrophic Cardiomyopathy: Insights From the NHLBI International HCM Registry. JACC Cardiovasc Imaging. 2022; doi: 10.1016/j.jcmg.2022.10.005.

65. Jia-Ning C, Ya-Nan Z, Wei W, Tao L. Associations of Infarct Size and Regional Myocardial Function Examined by Cardiac Magnetic Resonance Feature Tracking Strain Analysis with the Infarct Location in Patients with Acute ST-Segment Elevation Myocardial Infarction. Chin Med Sci J. 2022;37(4):309–319.

66. Gonzalez FA, Ângelo-Dias M, Martins C, et al. Left atrial strain is associated with distinct inflammatory and immune profile in patients with COVID-19 pneumonia. Ultrasound J. 2023;15(1):2.

67. Torpoco Rivera DM, Sriram C, Karpawich PP, Aggarwal S. Ventricular Functional Analysis in Congenital Complete Heart Block Using Speckle Tracking: Left Ventricular Epicardial Compared to Right Ventricular Septal Pacing. Pediatr Cardiol. 2023; doi: 10.1007/s00246-022-03093-7.

68. Wang F, Xu X, Wang Q, Yu D, Lv L, Wang Q. Comparison of left ventricular global and segmental strain parameters by cardiovascular magnetic resonance tissue tracking in light-chain cardiac amyloidosis and hypertrophic cardiomyopathy. Quant Imaging Med Surg. 2023;13(1):449–461.

69. Guo X, Liu M, Gong J, et al. Left ventricular strain in patients with Takayasu arteritis with preserved ejection fraction: an analysis using cardiac magnetic resonance imaging feature tracking. Quant Imaging Med Surg. 2023;13(1):171–184.

70. Sharifkazemi M, Nazarinia M, Arjangzade A, Goldust M, Hooshanginezhad Z. Diagnosis of Simultaneous Atrial and Ventricular Mechanical Performance in Patients with Systemic Sclerosis. Biology . 2022;11(2). doi: 10.3390/biology11020305.

71. Du Toit R, Herbst PG, van Rensburg A, du Plessis LM, Reuter H, Doubell AF. Clinical features and outcome of lupus myocarditis in the Western Cape, South Africa. Lupus. 2017;26(1):38–47.

72. Bai W, Xu R, Li X, et al. Prognostic value of cardiac magnetic resonance imaging parameters in left ventricular noncompaction with left ventricular dysfunction. BMC Cardiovasc Disord. 2022;22(1):526.

73. Endo K, Kiko T, Yamakuni R, et al. Prognostic Value of Simultaneous Analysis with Myocardial Flow Reserve and Right Ventricular Strain by Hybrid 13N-Ammonia Positron Emission Tomography/Magnetic Resonance Imaging in Coronary Artery Disease. Int Heart J. 2022;63(6):1063–1069.

74. Golukhova EZ, Alexandrova SA, Bulaeva NI, Mrikaev DV, Gromova OI, Berdibekov BS. Prognostic value of myocardial strain by magnetic resonance imaging in nonischemic dilated cardiomyopathy: a systematic review and meta-analysis. Kardiologiia. 2022;62(10):35–41.

75. Tantawy AAG, Elsherif NHK, Habeeb NM, Hasan EM, Abdelhameed AE. A two-dimensional speckle-tracking echocardiography for the diagnosis of early myocardial disease in beta-thalassemia major patients. Ann Pediatr Cardiol. 2022;15(3):257–265.

76. Liu W, Li W, Li H, et al. Two-dimensional speckle tracking echocardiography help identify breast cancer therapeutics-related cardiac dysfunction. BMC Cardiovasc Disord. 2022;22(1):548.

77. Chudgar PD, Burkule NJ, Kamat NV, Rege GM, Jantre MN. Myocardial Strain Imaging Using Feature Tracking Method of Cardiac MRI: Our Initial Experience of This Novel Parameter as an Additional Diagnostic Tool. Indian J Radiol Imaging. 2022;32(4):479–487.

78. Erley J, Starekova J, Sinn M, et al. Cardiac magnetic resonance feature tracking global and segmental strain in acute and chronic ST-elevation myocardial infarction. Sci Rep. 2022;12(1):22644.

79. Altiok E, Tiemann S, Becker M, et al. Myocardial deformation imaging by two-dimensional speckle-tracking echocardiography for prediction of global and segmental functional changes after acute myocardial infarction: a comparison with late gadolinium enhancement cardiac magnetic resonance. J Am Soc Echocardiogr. 2014;27(3):249–257.

80. Sharrack N, Das A, Kelly C, et al. The relationship between myocardial

microstructure and strain in chronic infarction using cardiovascular magnetic resonance diffusion tensor imaging and feature tracking. J Cardiovasc Magn Reson. 2022;24(1):66.

81. Guaricci AI, Chiarello G, Gherbesi E, et al. Coronary-specific quantification of myocardial deformation by strain echocardiography may disclose the culprit vessel in patients with non-ST-segment elevation acute coronary syndrome. Eur Heart J Open. 2022. p. oeac010.

82. Stathogiannis K, Mor-Avi V, Rashedi N, Lang RM, Patel AR. Regional myocardial strain by cardiac magnetic resonance feature tracking for detection of scar in ischemic heart disease. Magn Reson Imaging. 2020;68:190–196.

83. Weigand J, Nielsen JC, Sengupta PP, Sanz J, Srivastava S, Uppu S. Feature Tracking-Derived Peak Systolic Strain Compared to Late Gadolinium Enhancement in Troponin-Positive Myocarditis: A Case-Control Study. Pediatr Cardiol. 2016;37(4):696–703.

84. Ruivo C, Vilela EM, Ladeiras-Lopes R, Faria R, Ferreira N, Ribeiro VG. Myocardial deformation measures by cardiac magnetic resonance tissue tracking in myocarditis: Relationship with systolic function and myocardial damage. Rev Port Cardiol. 2019;38(11):767–776.

85. Hassan K, Doubell A, Kyriakakis C, et al. Comparing the findings and diagnostic sensitivity of cardiovascular magnetic resonance in biopsy confirmed acute myocarditis with infarct-like vs. heart failure presentation. J Cardiovasc Magn Reson. 2022;24(1):69.

86. Xie T, Zang X, Xiong Y, et al. Myoglobin and left ventricular ejection fraction as predictive markers for death in children with fulminant myocarditis. Front Pediatr. 2022;10:949628.

87. Akgül F, Er A, Ulusoy E, et al. Are clinical features and cardiac biomarkers at admission related to severity in pediatric acute myocarditis?: Clinical features and cardiac biomarkers in pediatric acute myocarditis. Arch Pediatr. 2022;29(5):376–380.

88. Gatti M, Palmisano A, Faletti R, et al. Two-dimensional and three-dimensional cardiac magnetic resonance feature-tracking myocardial strain analysis in acute

myocarditis patients with preserved ejection fraction. Int J Cardiovasc Imaging. 2019;35(6):1101–1109.

89. Luetkens JA, Petry P, Kuetting D, et al. Left and right ventricular strain in the course of acute myocarditis: a cardiovascular magnetic resonance study. Rofo. 2018;190(8):722–732.

90. Doerner J, Bunck AC, Michels G, Maintz D, Baeßler B. Incremental value of cardiovascular magnetic resonance feature tracking derived atrial and ventricular strain parameters in a comprehensive approach for the diagnosis of acute myocarditis. Eur J Radiol. 2018;104:120–128.

91. Baeßler B, Schaarschmidt F, Dick A, Michels G, Maintz D, Bunck AC. Diagnostic implications of magnetic resonance feature tracking derived myocardial strain parameters in acute myocarditis. Eur J Radiol. 2016;85(1):218–227.

92. Isaak A, Kravchenko D, Mesropyan N, et al. Layer-specific Strain Analysis with Cardiac MRI Feature Tracking in Acute Myocarditis. Radiol Cardiothorac Imaging. 2022;4(3):e210318.

93. Doimo S, Ricci F, Aung N, et al. Tissue-tracking in the assessment of late gadolinium enhancement in myocarditis and myocardial infarction. Magn Reson Imaging. 2020;73:62–69.

94. Uppu SC, Shah A, Weigand J, et al. Two-dimensional speckle-tracking-derived segmental peak systolic longitudinal strain identifies regional myocardial involvement in patients with myocarditis and normal global left ventricular systolic function. Pediatr Cardiol. 2015;36(5):950–959.

95. Chen X, Hu H, Pan J, Shu J, Hu Y, Yu R. Performance of cardiovascular magnetic resonance strain in patients with acute myocarditis. Cardiovasc Diagn Ther. 2020;10(4):725–737.

96. Meindl C, Paulus M, Poschenrieder F, Zeman F, Maier LS, Debl K. Patients with acute myocarditis and preserved systolic left ventricular function: comparison of global and regional longitudinal strain imaging by echocardiography with quantification of late gadolinium enhancement by CMR. Clin Res Cardiol. 2021;110(11):1792–1800.

97. Chinali M, Franceschini A, Ciancarella P, et al. Echocardiographic two-dimensional speckle tracking identifies acute regional myocardial edema and sub-acute fibrosis in pediatric focal myocarditis with normal ejection fraction: comparison with cardiac magnetic resonance. Sci Rep. 2020;10(1):11321.

98. Kostakou PM, Kostopoulos VS, Tryfou ES, et al. Subclinical left ventricular dysfunction and correlation with regional strain analysis in myocarditis with normal ejection fraction. A new diagnostic criterion. Int J Cardiol. 2018;259:116–121.

99. Poyraz E, Dinç Asarcıklı L. Dynamic Change of Left Ventricular Mechanics in Patients with Acute Myocarditis with Preserved Left Ventricular Systolic Function: A 2-Year Follow-up Study. Turk Kardiyol Dern Ars. 2022;50(7):485–491.

100. Truong DT, Dionne A, Muniz JC, et al. Clinically Suspected Myocarditis Temporally Related to COVID-19 Vaccination in Adolescents and Young Adults: Suspected Myocarditis After COVID-19 Vaccination. Circulation. 2022;145(5):345–356.

101. Vaidya Y, Cavanaugh SM, Dhamoon AS. Myocardial Stunning and Hibernation. StatPearls. Treasure Island (FL): StatPearls Publishing; 2022.

102. Flett AS, Hayward MP, Ashworth MT, et al. Equilibrium contrast cardiovascular magnetic resonance for the measurement of diffuse myocardial fibrosis: preliminary validation in humans. Circulation. 2010;122(2):138–144.

103. Nigri M, Azevedo CF, Rochitte CE, et al. Contrast-enhanced magnetic resonance imaging identifies focal regions of intramyocardial fibrosis in patients with severe aortic valve disease: Correlation with quantitative histopathology. Am Heart J. 2009;157(2):361–368.

104. Iles L, Pfluger H, Phrommintikul A, et al. Evaluation of diffuse myocardial fibrosis in heart failure with cardiac magnetic resonance contrast-enhanced T1 mapping. J Am Coll Cardiol. 2008;52(19):1574–1580.

105. Sibley CT, Noureldin RA, Gai N, et al. T1 Mapping in cardiomyopathy at cardiac MR: comparison with endomyocardial biopsy. Radiology. 2012;265(3):724–732.

106. Messroghli DR, Moon JC, Ferreira VM, et al. Clinical recommendations for cardiovascular magnetic resonance mapping of T1, T2, T2* and extracellular

volume: A consensus statement by the Society for Cardiovascular Magnetic Resonance (SCMR) endorsed by the European Association for Cardiovascular Imaging (EACVI). J Cardiovasc Magn Reson. 2017;19(1):75.

107. Karamitsos TD, Arvanitaki A, Karvounis H, Neubauer S, Ferreira VM. Myocardial Tissue Characterization and Fibrosis by Imaging. JACC Cardiovasc Imaging. 2020;13(5):1221–1234.

108. Goody PR, Zimmer S, Öztürk C, et al. 3D-speckle-tracking echocardiography correlates with cardiovascular magnetic resonance imaging diagnosis of acute myocarditis - An observational study. Int J Cardiol Heart Vasc. 2022;41:101081.

109. Luetkens JA, Homsi R, Dabir D, et al. Comprehensive Cardiac Magnetic Resonance for Short-Term Follow-Up in Acute Myocarditis. J Am Heart Assoc. 2016;5(7). doi: 10.1161/JAHA.116.003603.

110. López B, Ravassa S, Moreno MU, et al. Diffuse myocardial fibrosis: mechanisms, diagnosis and therapeutic approaches. Nat Rev Cardiol. 2021;18(7):479–498.

111. Pollack A, Kontorovich AR, Fuster V, Dec GW. Viral myocarditis--diagnosis, treatment options, and current controversies. Nat Rev Cardiol. 2015;12(11):670–680.

112. Baeßler B, Schaarschmidt F, Treutlein M, et al. Re-evaluation of a novel approach for quantitative myocardial oedema detection by analysing tissue inhomogeneity in acute myocarditis using T2-mapping. Eur Radiol. 2017;27(12):5169–5178.

113. Luetkens JA, Homsi R, Sprinkart AM, et al. Incremental value of quantitative CMR including parametric mapping for the diagnosis of acute myocarditis. Eur Heart J Cardiovasc Imaging. 2016;17(2):154–161.

114. Bohnen S, Radunski UK, Lund GK, et al. Tissue characterization by T1 and T2 mapping cardiovascular magnetic resonance imaging to monitor myocardial inflammation in healing myocarditis. Eur Heart J Cardiovasc Imaging. 2017;18(7):744–751.

115. Cokkinos DV, Pantos C. Myocardial remodeling, an overview. Heart Fail Rev. 2011;16(1):1–4.

116. Vermes E, Childs H, Faris P, Friedrich MG. Predictive value of CMR criteria for LV functional improvement in patients with acute myocarditis. Eur Heart J Cardiovasc Imaging. 2014;15(10):1140–1144.

117. Raziyeva K, Smagulova A, Kim Y, Smagul S, Nurkesh A, Saparov A. Preconditioned and Genetically Modified Stem Cells for Myocardial Infarction Treatment. Int J Mol Sci. 2020;21(19). doi: 10.3390/ijms21197301.

118. Golpanian S, Wolf A, Hatzistergos KE, Hare JM. Rebuilding the Damaged Heart: Mesenchymal Stem Cells, Cell-Based Therapy, and Engineered Heart Tissue. Physiol Rev. 2016;96(3):1127–1168.

119. Karantalis V, Balkan W, Schulman IH, Hatzistergos KE, Hare JM. Cell-based therapy for prevention and reversal of myocardial remodeling. Am J Physiol Heart Circ Physiol. 2012;303(3):H256–H270.

120. Karantalis V, Hare JM. Use of mesenchymal stem cells for therapy of cardiac disease. Circ Res. 2015;116(8):1413–1430.

121. Qayyum AA, van Klarenbosch B, Frljak S, et al. Effect of allogeneic adipose tissue-derived mesenchymal stromal cell treatment in chronic ischaemic heart failure with reduced ejection fraction - the SCIENCE trial. Eur J Heart Fail. 2023; doi: 10.1002/ejhf.2772.

122. Qayyum AA, Mouridsen M, Nilsson B, et al. Danish phase II trial using adipose tissue derived mesenchymal stromal cells for patients with ischaemic heart failure. ESC Heart Fail. 2023; doi: 10.1002/ehf2.14281.

123. Wu M, Pelacho B, Claus P, et al. Alginate Sulfate-Nanoparticles Loaded with Hepatocyte Growth Factor and Insulin-Like Growth Factor-1 Improve left ventricular repair in a Porcine Model of Myocardial Ischemia Reperfusion Injury. Eur J Pharm Biopharm. 2023; doi: 10.1016/j.ejpb.2023.01.012.

124. Qayyum AA, Mathiasen AB, Helqvist S, et al. Autologous adipose-derived stromal cell treatment for patients with refractory angina (MyStromalCell Trial): 3-years follow-up results. J Transl Med. 2019;17(1):360.

125. Toma C, Pittenger MF, Cahill KS, Byrne BJ, Kessler PD. Human mesenchymal stem cells differentiate to a cardiomyocyte phenotype in the adult murine heart.

Circulation. 2002;105(1):93–98.

126. Amado LC, Saliaris AP, Schuleri KH, et al. Cardiac repair with intramyocardial injection of allogeneic mesenchymal stem cells after myocardial infarction. Proc Natl Acad Sci U S A. 2005;102(32):11474–11479.

127. Hamamoto H, Gorman JH 3rd, Ryan LP, et al. Allogeneic mesenchymal precursor cell therapy to limit remodeling after myocardial infarction: the effect of cell dosage. Ann Thorac Surg. 2009;87(3):794–801.

128. Silva GV, Litovsky S, Assad JAR, et al. Mesenchymal stem cells differentiate into an endothelial phenotype, enhance vascular density, and improve heart function in a canine chronic ischemia model. Circulation. 2005;111(2):150–156.

129. Mathiasen AB, Qayyum AA, Jørgensen E, et al. Bone marrow-derived mesenchymal stromal cell treatment in patients with ischaemic heart failure: final 4-year follow-up of the MSC-HF trial. Eur J Heart Fail. 2020;22(5):884–892.

130. Mathiasen AB, Qayyum AA, Jørgensen E, et al. Bone marrow-derived mesenchymal stromal cell treatment in patients with severe ischaemic heart failure: a randomized placebo-controlled trial (MSC-HF trial). Eur Heart J. 2015;36(27):1744–1753.

131. Tompkins BA, Rieger AC, Florea V, et al. Comparison of Mesenchymal Stem Cell Efficacy in Ischemic Versus Nonischemic Dilated Cardiomyopathy. J Am Heart Assoc. 2018;7(14). doi: 10.1161/JAHA.117.008460.

132. Hare JM, DiFede DL, Rieger AC, et al. Randomized Comparison of Allogeneic Versus Autologous Mesenchymal Stem Cells for Nonischemic Dilated Cardiomyopathy: POSEIDON-DCM Trial. J Am Coll Cardiol. 2017;69(5):526–537.

133. Ankrum JA, Ong JF, Karp JM. Mesenchymal stem cells: immune evasive, not immune privileged. Nat Biotechnol. 2014;32(3):252–260.

134. Andrzejewska A, Lukomska B, Janowski M. Concise Review: Mesenchymal Stem Cells: From Roots to Boost. Stem Cells. 2019;37(7):855–864.

135. Kim PK, Hong YJ, Im DJ, et al. Myocardial T1 and T2 Mapping: Techniques and Clinical Applications. Korean J Radiol. 2017;18(1):113–131.

136. Küstner T, Bustin A, Jaubert O, et al. Isotropic 3D Cartesian single breath-hold CINE MRI with multi-bin patch-based low-rank reconstruction. Magn Reson Med. 2020;84(4):2018–2033.

137. Nordio G, Bustin A, Henningsson M, et al. 3D SASHA myocardial T1 mapping with high accuracy and improved precision. MAGMA. 2019;32(2):281–289.

138. Ferreira da Silva T, Galan-Arriola C, Montesinos P, et al. Single breath-hold saturation recovery 3D cardiac T1 mapping via compressed SENSE at 3T. MAGMA. 2020;33(6):865–876.

139. Røsner A, Alessandrini M, Kjønås D, Mirea O, Queirós S, D Hooge J. Quality Assurance of Segmental Strain Values Provided by Commercial 2-D Speckle Tracking Echocardiography Using in Silico Models: A Report from the EACVI-ASE Strain Standardization Task Force. Ultrasound Med Biol. 2021;47(11):3079–3089.

# A Appendix

# I List of abbreviations

| | | |
|---|---|---|
| AHA | = | American Heart Association |
| ASC | = | adipose-derived stromal cells |
| AV | = | atrioventricular |
| bSSFP | = | balanced steady-state free precession |
| CI | = | confidence interval |
| circ | = | circumferential |
| CK-MB | = | creatine kinase of the myocardium |
| COVID-19 | = | coronavirus disease 2019 |
| CT | = | computer tomography |
| DCM | = | dilated cardiomyopathy |
| ECG | = | electrocardiogram |
| ECV | = | extracellular volume |
| ED | = | end-diastolic |
| EGE | = | early gadolinium enhancement |
| EMB | = | endomyocardial biopsy |
| ES | = | end-systolic |
| ESC | = | European Society of Cardiology |
| EU | = | Erstuntersuchung |
| FT | = | feature tracking |
| FU | = | follow-up/Folgeuntersuchung |
| HFrEF | = | heart failure with reduced ejection fraction |
| HIV-1 | = | human immunodeficiency virus-1 |
| Int. | = | interaction |
| LAX | = | long axes |
| LGE | = | late gadolinium enhancement |
| LLC | = | Lake Louise Criteria |
| long | = | longitudinal |
| LR test | = | likelihood ratio test |
| LV | = | left ventricle/left ventricular/linksventrikulär |
| LVAD | = | left ventricular assist devices |
| (LV)EF | = | (left ventricular) ejection fraction |
| MOLLI | = | modified Look-Locker inversion recovery |
| MRI | = | magnetic resonance imaging |

| | | |
|---|---|---|
| MRT | = | Magnetresonanztomographie |
| MSC | = | mesenchymal stromal cells |
| NT-proBNP | = | N-terminal pro–B-type natriuretic peptide |
| NYHA | = | New York Heart Association |
| PCR | = | polymerase chain reaction |
| POSEIDON-DCM | = | Percutaneous Stem Cell Injection Delivery Effects on Neomyogenesis in Dilated Cardiomyopathy |
| rad | = | radial |
| Reg. coef. | = | regression coefficient |
| RV | = | right ventricle |
| SARS-CoV-2 | = | severe acute respiratory syndrome coronavirus 2 |
| SAX | = | short axis |
| SD | = | standard deviation |
| SRPS_SAX | = | segmental radial peak strain in short axis view |
| STIR | = | short tau inversion recovery |
| TE | = | echo time |
| TI | = | inversion recovery time |
| TR | = | repetition time |
| VA-ECMO | = | veno-arterial extracorporeal membrane oxygenation |
| ΔT | = | relaxation time at follow-up minus relaxation time at baseline |
| 2Ch | = | 2-chamber |
| 4Ch | = | 4-chamber |

# II List of figures

# III List of tables